Spent Fuel Matrix Degradation and Canister Corrosion: Quantifying the Effect of Hydrogen

Spent Fuel and Waste Disposition

Prepared for
US Department of Energy
Spent Fuel and Waste Science and Technology
James Jerden
Kurt Frey
William Ebert
Argonne National Laboratory
February 28, 2017
SFWD-SFWST-2017-000039
SFWD-SFWST-2017-000042

This work was supported by the US Department of Energy, Office of Nuclear Energy. The report was prepared at Argonne National Laboratory as part of the Spent Fuel and Waste Science and Technology Campaign.

ABSTRACT

It has been shown in both experimental and modeling studies that H_2 plays the dominant role in determining the fuel dissolution rate and even moderate concentrations of H_2 suppress the oxidative dissolution of spent fuel. The major source of H_2 within a breached waste package in low-oxygen environments will be anoxic corrosion of the various steels used as containers and structural components. The steel corrosion and H_2 generation reactions are coupled redox reactions and the rates are equal under anoxic conditions. Therefore, a steel corrosion model has been added to the fuel matrix degradation model (FMDM) as the kinetic source of H_2 (and Fe^{2+}). Once it is fully calibrated, the steel corrosion model will be used to calculate the corrosion rates of various metals under the environmental conditions in a breached waste package as a function of temperature, Eh, pH and solution chemistry to provide the H_2 concentrations controlling the fuel degradation rate. This report identifies the processes through which steel corrosion is coupled with the fuel degradation kinetics in the FMDM and summarizes the sensitivity of the calculated fuel degradation rate to the range of corrosion rates relevant for different steels expected to be present in a waste package. It also identifies information gaps that need to be filled in order to further develop, parameterize, and calibrate the steel corrosion model.

EXECUTIVE SUMMARY

This work is being performed as part of the DOE NE Spent Fuel and Waste Science and Technology Campaign Argillite and Crystalline Rock R&D work packages: SF-17AN01030103 and SF-17AN01030203. This document meets the February 28, 2017 milestone ANL M3SF-17AN010301031 for Argillite R&D and the February 28, 2017 milestone M3SF-17AN010302031 for Crystalline R&D.

Overall, the purpose of this project is to develop a process model based on fundamental thermodynamics, kinetics and electrochemistry to calculate the degradation rate of spent UO_2 fuel that can be integrated in the generic disposal system analysis (GDSA) performance assessment (PA) model. The focus of on-going work is to accurately and quantitatively represent the effect of H_2 on the long-term degradation rate of the spent fuel. It has been shown experimentally that even moderate concentrations of H_2 in solution can inhibit the oxidative degradation and that fuel degradation rates can decrease by as much as 4 orders of magnitude when H_2 is present at high concentrations. A recent sensitivity study showed the dissolved H_2 concentration is the dominant environmental variable affecting the UO_2 fuel dissolution rate (Jerden et al., 2015). Most of the H_2 in disposal systems will be generated by radiolysis and anoxic corrosion of metallic engineering materials, including stainless steel containers, carbon steel spacers, and Zircaloy cladding. Therefore, a simple steel corrosion module has been added to the fuel matrix degradation model (FMDM) to couple the H_2 generation and fuel degradation processes and evaluate the sensitivity of fuel degradation rates to steel corrosion rates using the FMDM. Modeling runs using ranges of measured steel corrosion rates indicate the corrosion of steel components will generate sufficient H_2 to attenuate peak rates and radionuclide source terms. The information flow from the performance assessment model (PA) to the FMDM and back to the PA is summarized in Figure 1. It is important to note that the steel and fuel corrosion rates must be calculated for the same environmental conditions (and depend on many of the same variables), and that the diffusion of H_2 and radiolysis products between the steel and fuel surfaces is taken into account in the coupled reactions. Note also that PA provides the initial composition of water entering the breached package, but the in-package solution evolves within the FMDM as steel and fuel degrade.

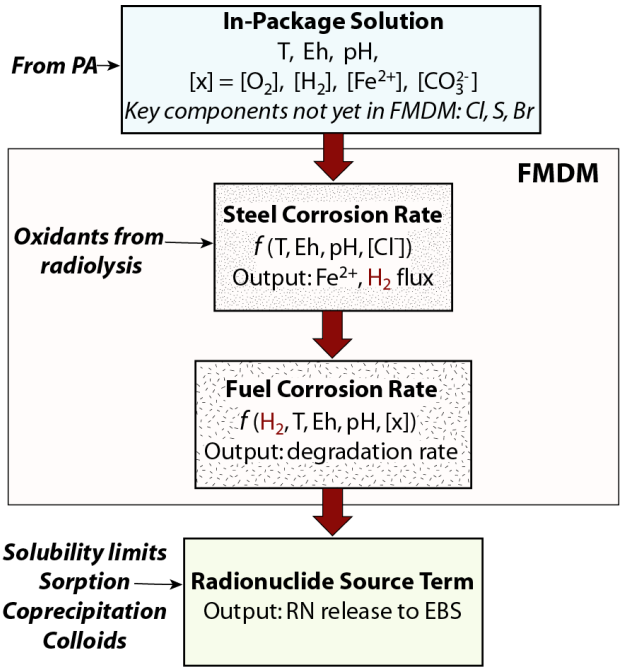

Summary figure showing the context of the FMDM within the source term calculation information flow

Analysis of these sensitivity calculations identified several information gaps that need to be filled to calibrate and validate the coupled fuel matrix degradation - steel corrosion model. The highest priority information gaps are as follows:

- A wide range of steel corrosion rates have been derived from measured mass loss in coupon immersion tests. Whereas those tests can be used to derive average rates under uncontrolled conditions, they do not provide the dependencies on environmental variables required to calculate accurate spent fuel dissolution rates. Most importantly, the dependencies of the steel corrosion rates on Eh and pH and the attenuating effect of passivation must be known to calibrate and validate the FMDM. Electrochemical methods have been developed at ANL to monitor the effects of key variables such as Eh, pH, and Cl^- concentration on the long-term corrosion rates of metals that corrode actively or passivate. These electrochemical corrosion rates are appropriate for calculating H_2 generation with the FMDM steel corrosion model.

- Steel corrosion is modeled using the same mixed potential theory that is the basis of fuel degradation in the FMDM and the electrochemically coupled reactions contributing to steel corrosion and UO_2 fuel degradation have been included in FMDM V.3. While the simple steel corrosion model that has been implemented is sufficient to assess sensitivities, there remains a need for coupled experimental and process modeling work to implement, accurately parameterize and validate a more realistic steel corrosion module and its coupling to the fuel degradation model. Improvements to the process models used in the FMDM will have a direct impact on the accuracy of GDSA PA model results.

- Quantification of interactions between the corrosion of steel waste package components and waste form degradation would provide important insights as to the types of steel that could be used to optimize the long-term performance of the waste package and canister materials. For example, using a combination of actively corroding and passive metals having a range of corrosion rates could be utilized to generate H_2 throughout most of the regulated service life. The steel corrosion model developed to quantify H_2 generation within a breach waste package can also be used to model external corrosion kinetics in bentonite pore water and possibly model container breaching.

- The sensitivity runs performed with the FMDM indicate that oxidants and reductants (most importantly H_2) accumulate in porous alteration products that form on the fuel surface and significantly affect the fuel degradation rate. Whether this process actually occurs or is an artifact of the model must be determined experimentally.

- The FMDM uses kinetic parameters for individual reactions that were measured in tests with UO_2. Based on the use of robust canisters, it is likely that much of the spent fuel in a repository will not be contacted by groundwater until canisters begin to fail more than 1000 years after repository closure. More studies are needed to determine the effects of aging on fuel dissolution rates by measuring dissolution rates of actinide oxide materials that simulate "aged" ~1000 yr old fuel in the presence of H_2. Such materials can be synthesized by doping UO_2 with fission product salts and actinides. Electrochemical tests to measure the dissolution rates of materials representing aged fuel alone and in the presence of corroding steel will provide the dataset required for reliable model validation add confidence to predictions of long-term rates.

This page is intentionally left blank.

This page is intentionally left blank.

LIST OF FIGURES

LIST OF TABLES

ACRONYMS

BWR	Boiling Water Reactor
DOE	U.S. Department of Energy
FEPs	Features, events, and processes
FMD	Fuel matrix degradation (model)
FMDM	Fuel matrix degradation model
GDSA	Generic Disposal System Analyses
ICP-MS	Inductively coupled plasma-mass spectrometry
MCNPX	Monte Carlo N-Particle eXtended
ORNL	Oak Ridge National Laboratory
PA	Performance assessment
R&D	Research and development
SEM	Scanning electron microscopy
SHE	Standard hydrogen electrode
SFWS	Spent Fuel and Waste Science and Technology (campaign)
SNF	Spent nuclear fuel
STAD	Standardized Transportation, Aging and Disposal Canister

This page is intentionally left blank.

SPENT FUEL AND WASTE SCIENCE AND TECHNOLOGY CAMPAIGN

1. INTRODUCTION AND OBJECTIVE

Scientifically-based predictive models of waste form corrosion rates are being developed to provide reliable radionuclide source terms for use in repository performance assessments. Furthermore, demonstrating that there is a fundamental scientific basis for the waste form degradation models is a key aspect for building confidence in the long-term predictions used for the repository safety case.

The objective of this project is to develop and implement a fundamentals-based process model for the degradation rate of spent nuclear fuel that can be readily incorporated into the Generic Disposal System Analyses (GDSA) Performance Assessment (PA) code to provide reliable radionuclide source terms throughout the service life of a repository. This model, referred to as the Fuel Matrix Degradation Model (FMDM), is based on the Canadian Mixed Potential Model (King and Kolar, 2003), but has been expanded and customized for application in the ongoing Spent Fuel and Waste Science and Technology (SFWS) campaign. The conceptual context for the role of the FMDM within the generic performance assessment model is shown in Figure 1. The FMDM will be used to calculate the degradation rate of UO_2 fuel under the environmental conditions in a breached waste package. The degradation rate will be used to calculate radionuclide source term values for use in reactive transport calculations through the EBS and host geology to demonstrate regulated dose limits will be met throughout the service life of the repository.

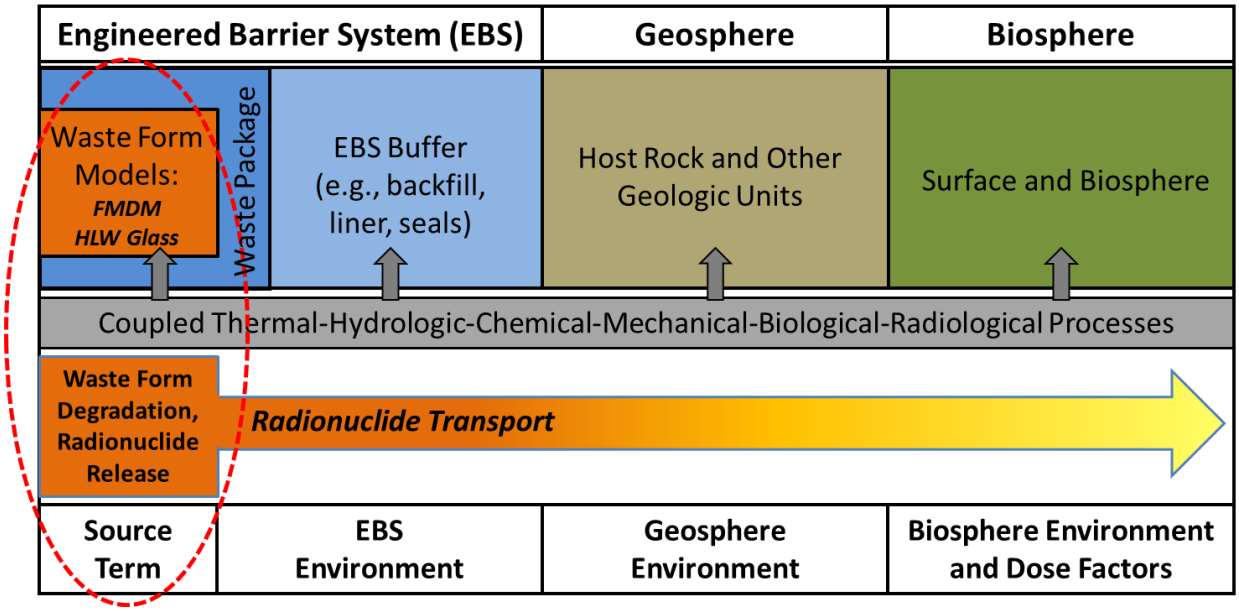

Figure 1. Conceptual diagram showing the context for the FMDM (adapted from Mariner et al., 2015).

The continuing development and implementation of the FMDM address two high level Features, Events, and Processes (FEPs) that are recognized as high R&D priorities for the SFWS campaign (Wang et al., 2014). The FEPs addressed by this model are 2.1.02 (waste form) and 2.1.03 (waste container), which correspond to the high priority research topics P19 (Development of waste form degradation model) and P20 (Development of new waste package concepts and models for evaluation of waste package performance for long-term disposal) identified by Wang et al., 2014.

The FMDM calculates the dissolution rate of spent fuel as a function of the interfacial corrosion potential (E_{corr}), at which all of the anodic and cathodic half reactions occurring at the fuel/solution boundary under the environmental conditions are kinetically balanced and there is no net electron transfer. The dissolution rate (which generates an anodic current due to the oxidation of U^{4+} to U^{6+}) is relatively high under oxidizing conditions above the U(IV)/U(VI) threshold potential, but significantly lower at E_{corr} values where only solubility-limited chemical dissolution of U^{4+} occurs. The threshold potential for U(IV)/U(VI) oxidative dissolution depends on pH, as shown in Figure 2, and on the water chemistry. Under the reducing conditions envisioned in argillite and crystalline rock repositories (the red region in Figure 2), the Eh of the solution will be well below the U(IV)/U(VI) threshold. However, the radiolysis of water by spent fuel to form H_2O_2 and O_2 can cause localized oxidizing conditions that drive the Eh above the threshold for oxidative dissolution of the fuel.

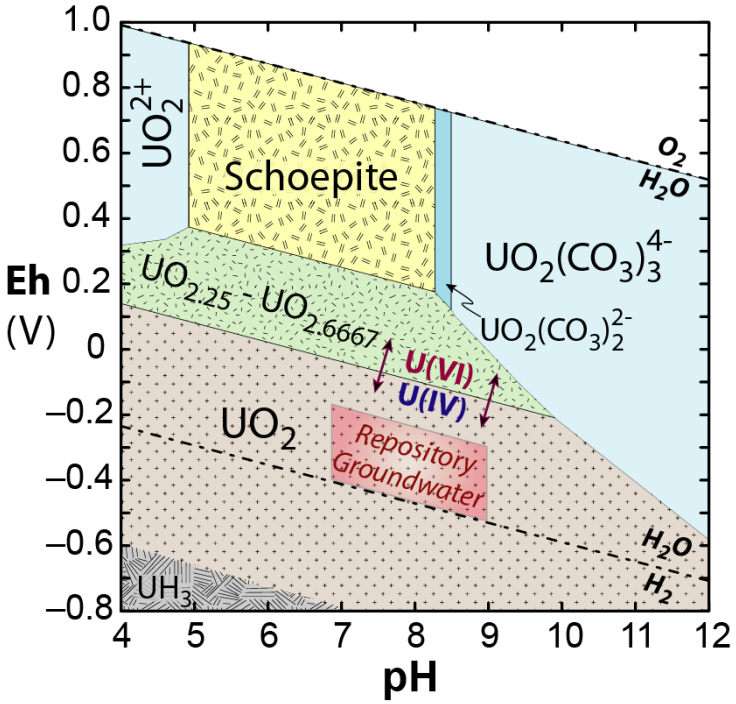

Figure 2. Eh – pH diagram for U speciation showing the conditions expected for groundwaters in a reducing crystalline rock or argillite repository (from Laaksoharju, et al., 2008). This diagram was drawn for $1x10^{-6}$ molar uranium with $1x10^{-4}$ molar carbonate.

A number of experimental and modeling studies have shown that the radiolytic oxidative dissolution of spent fuel in anoxic environments can be counteracted by the catalyzed reaction of H_2 on fission product alloy phases referred to as Ru ε-phases or noble metal particles (NMP). What we refer to as the H_2 effect has been shown qualitatively to decrease spent fuel dissolution rates by 3 to 4 orders of magnitude from the maximum rates attained in the absence of H_2, so it must be taken into account in scientifically based performance assessment calculations (e.g., Shoesmith, 2008, Grambow, et al., 2010, Jerden et al., 2015). The major goal of the ongoing FMDM work is to implement an accurate model that **quantifies** the H_2 effect on spent fuel degradation rates. This report presents results from a new version of the FMDM (V3) that incorporates a module for calculating the anoxic corrosion rates of steels as the main source of H_2 in a breached waste package and near field environment.

2. THE FUEL MATRIX DEGREDATION MODEL

The key processes represented in FMDM.V3 are:

- the generation of radiolytic oxidants as a function of fuel burn-up,
- the NMP-catalyzed oxidation of H_2, which protects the fuel from oxidative dissolution,
- the precipitation of U-bearing secondary phases,
- the complexation of uranyl by carbonate,
- the oxidation of ferrous iron,
- temperature variations of reaction rates (by Arrhenius equations),
- the one-dimensional diffusion of all chemical species to and from the fuel and steel surfaces,
- the anoxic corrosion of steel components to generate dissolved H_2 and ferrous iron.

Of these processes, the catalysis of H_2 oxidation on noble metal particles (NMP) exposed at the fuel surface and the generation rates of radiolytic oxidants (determined by dose rate, which is calculated in the FMDM based on fuel burn-up) are the most important for determining the degradation rate of the fuel (Jerden et al., 2015). Since the flux of H_2 to the fuel is limited by the anoxic corrosion rate of steel waste package components (e.g., Shoesmith, 2008), an initial module to calculate steel corrosion kinetics was added to the FMDM in FY-2016 to quantify the H_2 source concentration. The electrochemical steel corrosion module is discussed in Section 3.

Specifically, the fuel degradation rate calculated by the FMDM accounts for oxidation of the fuel by radiolytic H_2O_2 and its decomposition product O_2. The H_2O_2 concentration is calculated using an analytical form of the radiolysis model developed at PNNL (Buck et al., 2014) and the burn-up/dose rate function. Fuel oxidation is counteracted by the catalytic oxidation of H_2 on NMP sites that are present on the fuel surface as a distinct phase. The FMDM calculates the net effect of all redox reactions occurring in the system on the value of Ecorr at the fuel surface to determine the fuel dissolution rate.

In the absence of oxidative dissolution, the fuel degrades by solubility-limited chemical dissolution, which is much slower than oxidative dissolution (Figure 3, Röllin et al., 2001). It was shown in Jerden et al., 2015 that the FMDM accurately reproduces the experimental observation that relatively low concentrations of dissolved H_2 (~0.1 mM) can measurably inhibit the oxidative dissolution of the fuel. Those calculations were made with a range of user-defined H_2 concentrations. The steel corrosion module was added to calculate H_2 concentrations within the model. A simple initial model was used to couple the steel and fuel reactions and determine the sensitivity of the coupled rates. Based on these sensitivity results, a new model is being developed to calculate steel corrosion rates as a function of the environmental conditions.

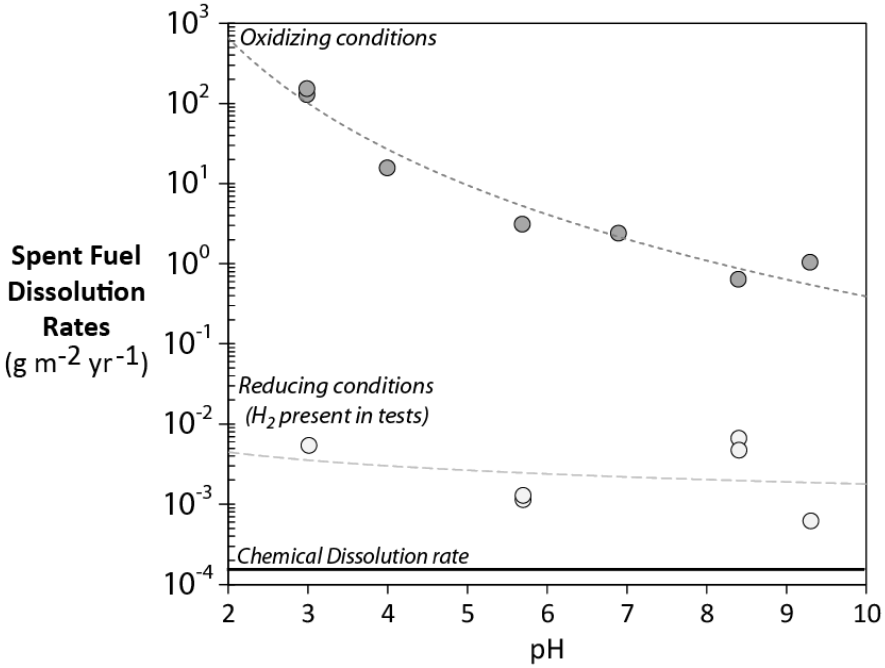

Figure 3. Results from the flow-through spent fuel dissolution tests of Röllin et al., 2001. Note that the rates measured in tests performed under reducing conditions with H_2 present are around 3 orders of magnitude lower than those in tests performed under oxidizing conditions at the same pH, but still higher than the chemical dissolution rate.

Figures 4 - 9 are simplified conceptual diagrams of a typical spent fuel canister in a repository setting. These figures highlight the spatial context and key processes that the FMDM takes into account. As shown in Figures 4 and 5, the spent fuel assemblies will be surrounded by (and in close contact with) steel components within the waste package and disposal canister, which may include low carbon steels (C-steel), borated stainless steels and 316 stainless steels. Another important material from the prospective of H_2 production in the repository is the Zircaloy cladding surrounding the fuel pellets (gold or yellow in Figures 4 – 7). No credit is taken for Zircaloy as a barrier in the current FMDM or GDSA PA models, but it will probably be beneficial to include Zircaloy corrosion as a source of H_2 the FMDM. This is discussed in more detail in Section 6.

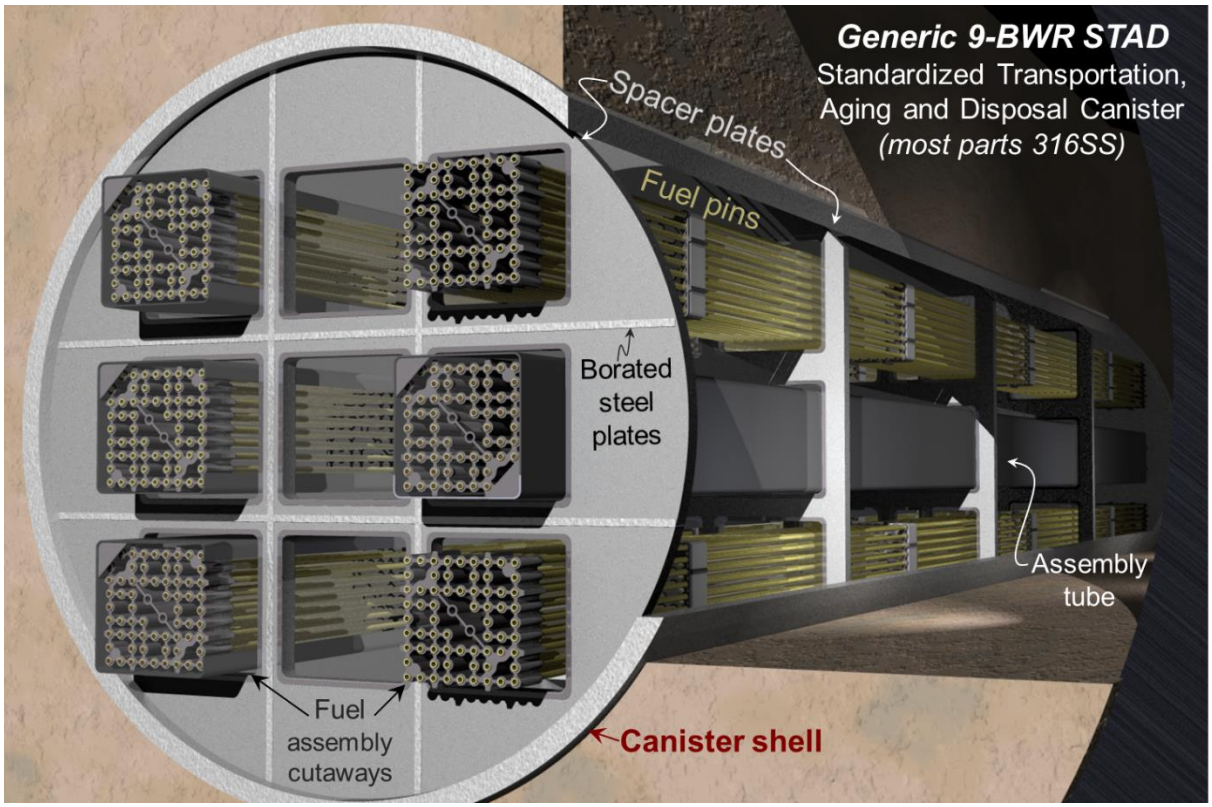

Figure 4. Conceptual diagram showing a generic BWR waste package (adapted from Energy Solutions, 2015).

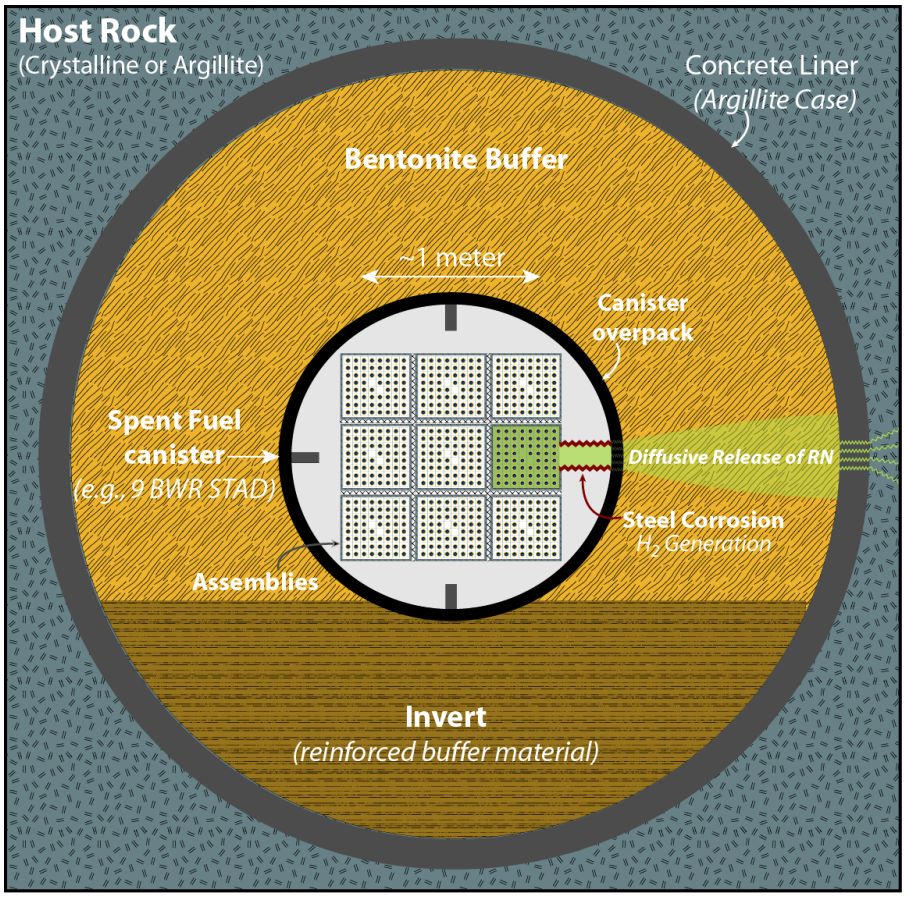

Figure 5. Conceptual diagram of a generic waste package showing a conceptual canister-breaching scenario. BWR STAD denotes a boiling water reactor standard transport, aging and disposal canister and RN denotes radionuclides.

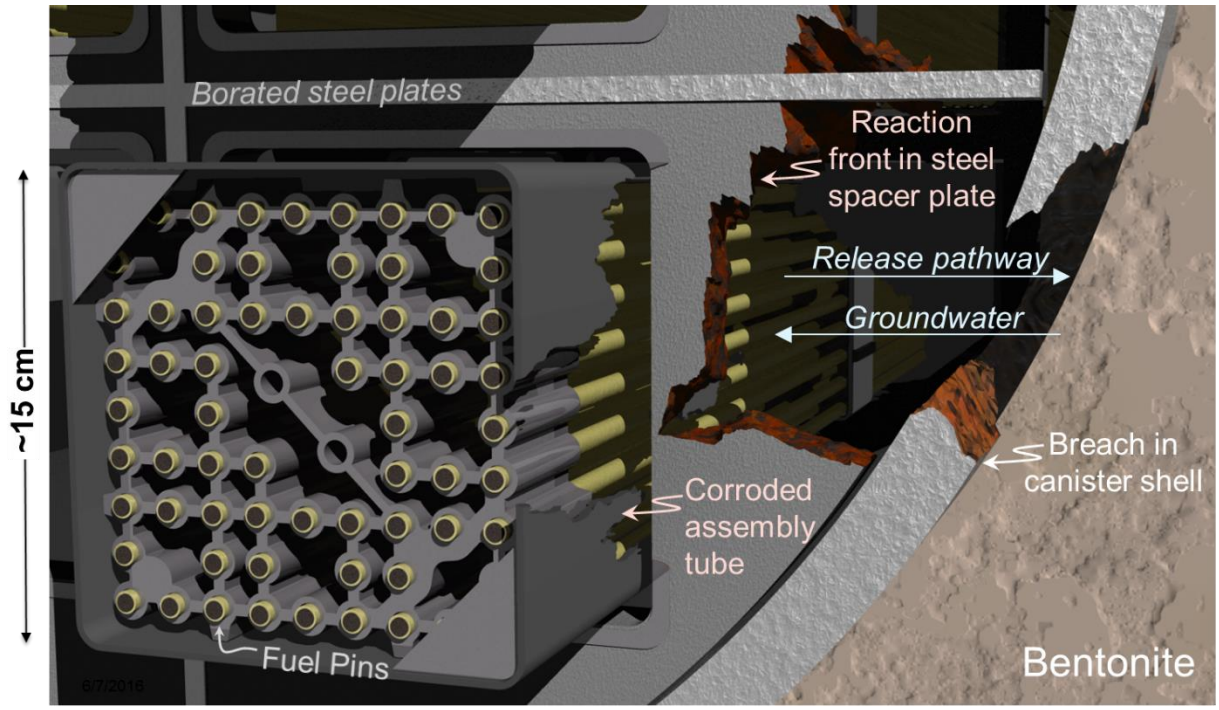

Figure 6. Conceptual diagram summarizing the key processes involved in radionuclide release from a breached spent fuel canister. Following a breach, seepage water will oxidize steel components and eventually reach fuel rods. Note that the fuel will degrade simultaneously with a number of different types of steels. The interactions with steel corrosion reaction products H_2 and Fe^{2+} have been shown to strongly affect the rate of fuel degradation (e.g., Shoesmith, 2008, Grambow, et al., 2010).

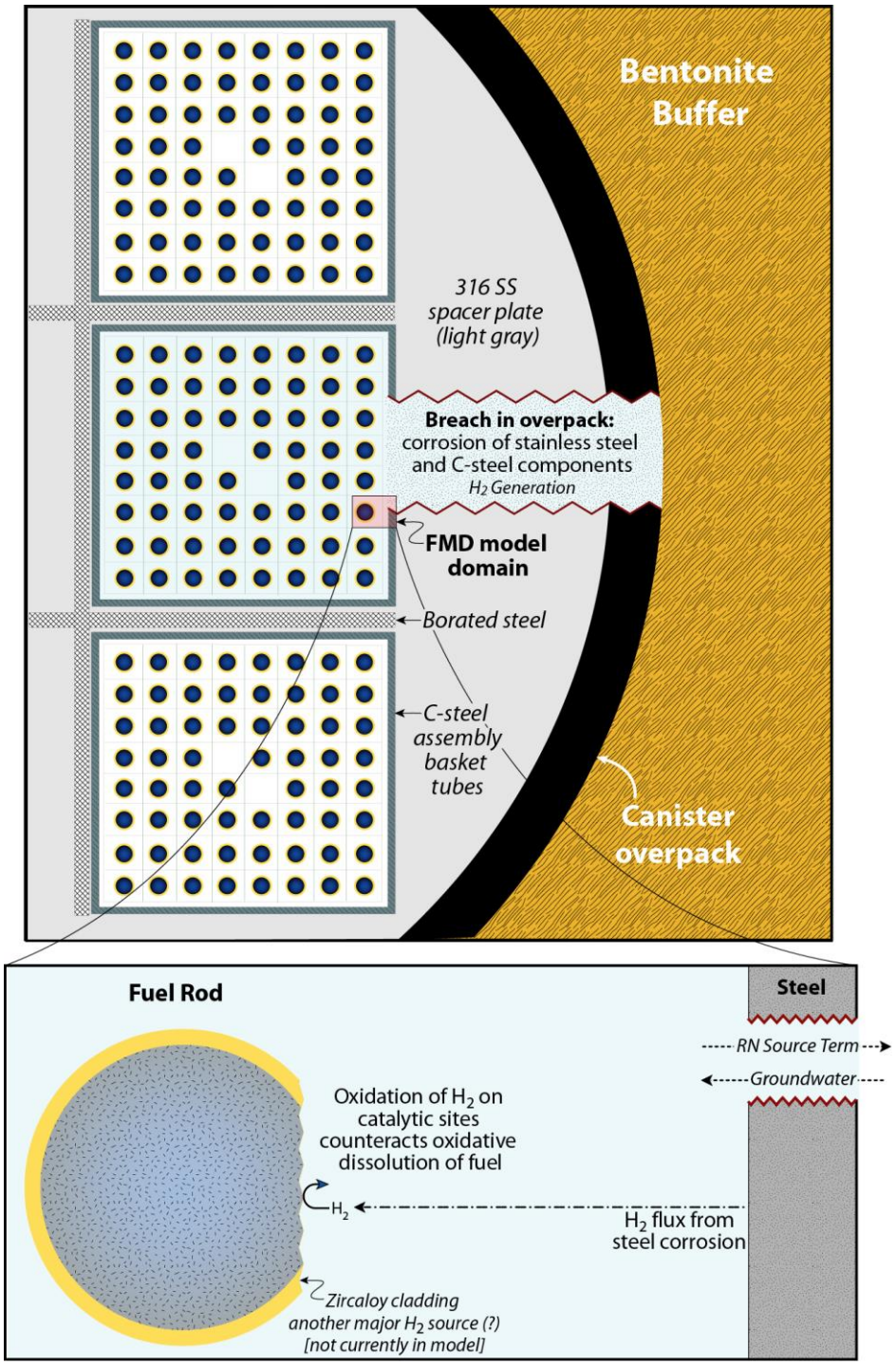

Figure 7. Conceptual diagram showing a generic BWR waste package and the conceptual context and lay-out of the fuel matrix degradation model (FMDM).

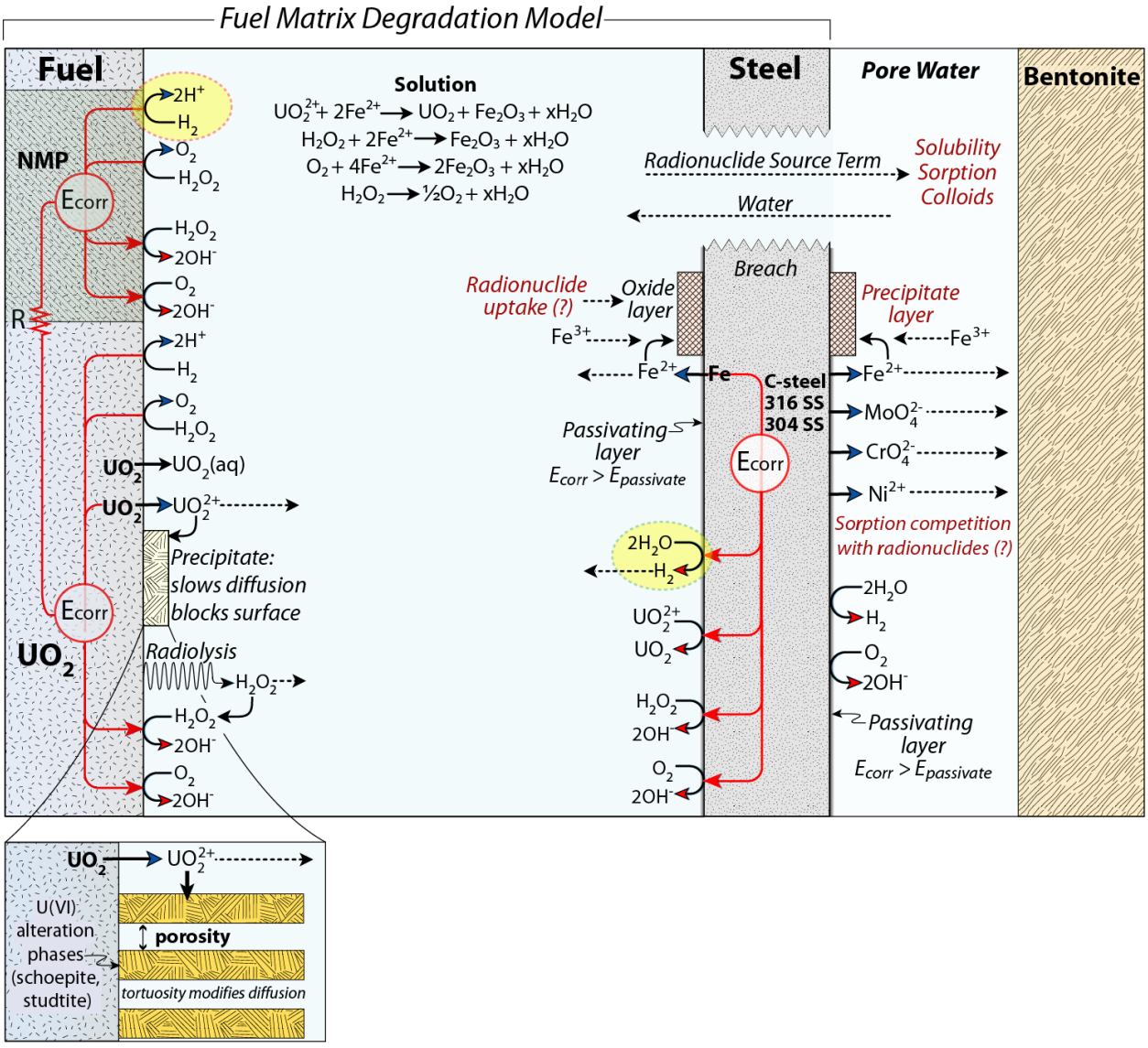

Figure 8. Schematic showing the reaction scheme for the fuel matrix degradation model and identifying other key processes that influence in-package chemistry and radionuclide mobilization. This report focuses on the reactions that are highlighted in yellow: H_2 generation during steel corrosion and H_2 oxidation on the fuel surface.

In a breached waste package, groundwater will infiltrate open spaces within the canister and begin to corrode steel components (Figure 6). This will set up a reaction front that will eventually contact the fuel rods. The steel will corrode and produce H_2 even when the infiltrating groundwaters are reducing with respect to the fuel. This is because the stability fields of carbon steels and stainless steels lie below the stability field of water (Figure 9). Assuming that the Zircaloy cladding has failed, the fuel will begin degrading by either relatively rapid oxidative dissolution or by relatively slow chemical dissolution, depending on the Eh and pH. The dominant dissolution mechanism will be determined by the surface potential established by the solution contacting the fuel surface. The FMDM employs fundamental electro-kinetic relationships (Butler-Volmer equations) and classical 1-D reaction-diffusion relationships to calculate the surface potential (E_{corr}) and corresponding spent fuel dissolution rate.

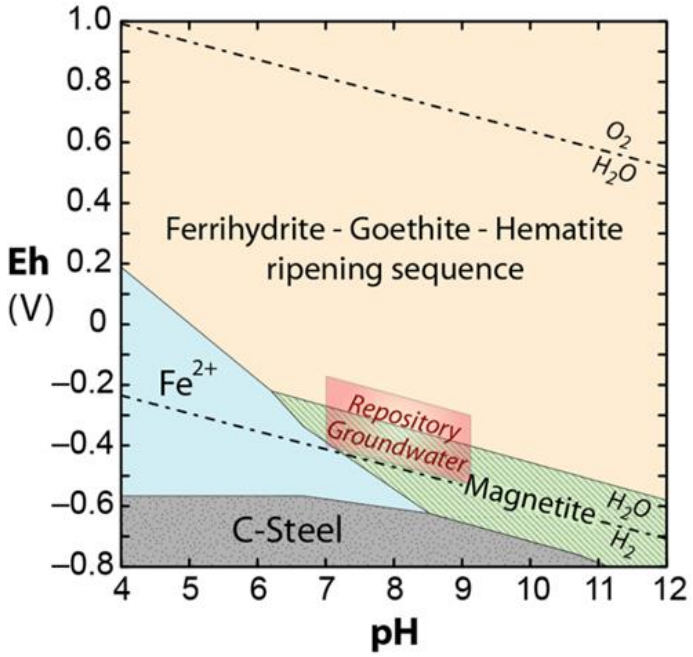

Figure 9. Eh – pH diagram showing the conditions expected for groundwaters in a reducing crystalline rock or argillite repository (from Laaksoharju, et al., 2008), drawn for $1x10^{-3}$ molar iron.

The mixed potential theory on which the FMDM is based is also used to quantify steel corrosion. Because it accounts for the fundamental interfacial electrochemical reactions and couples those reactions with bulk solution chemistry, it can be used to couple fuel dissolution and steel corrosion in a common seepage water. Therefore, as part of our FY-2016 work, we coded and tested a relatively simple mixed potential model for steel corrosion and then added that as a new module to the FMDM. This steel corrosion mixed potential model is based on the model presented by King and Kolar, 2001 and King and Kolar, 2003. The steel corrosion model is based on the Butler-Volmer model, but modified to account for passivation. The interfaces between the modules are presented schematically in Figure 10.

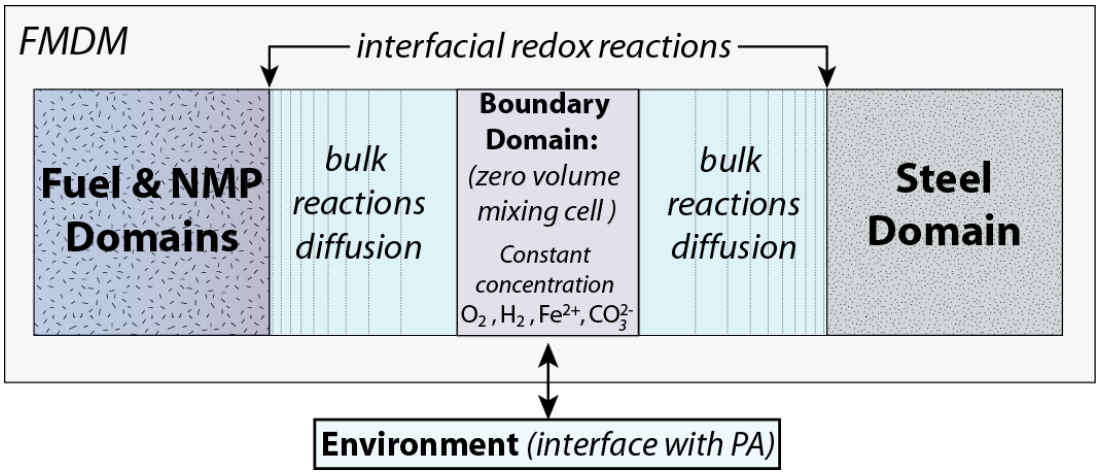

Figure 10. Schematic diagram showing how steel surface corrosion is represented in the FMDM.

As shown in Figure 10, the steel environment (steel surface plus bulk solution) is coupled to the fuel environment through a zero-volume interstitial domain (boundary mixing cell) that is used to exchange

mass fluxes between the fuel and steel through the seepage water in the breached waste package and with pore water in the adjacent near field environment. No chemistry occurs in the interstitial domain or environment; those regions are zero-volume and only serve to provide an interface between the fuel and steel domains used to model diffusion. It is possible to control the interaction between the steel and fuel domains by altering (1) the environmental concentrations, (2) the relative areas of the two reactive domains, and (3) the leak rate from the interstitial domain into the near field environment. The boundary cell serves as the input/output interface with the GDSA performance assessment model.

In parallel with the addition of the steel surface to the FMDM, the model parameter database was reviewed and updated. As part of this updating process, several data gaps were identified that provide priorities for future work. The main FMDM parameters and the important data gaps are summarized in Table 1.

The rate of fuel degradation will ultimately be determined by the kinetic balance of five processes (shown schematically in Figure 8):

- The rate of radiolytic oxidant production (determined by dose rate, which is determined by fuel burn up and age)
- The rate of radiolytic oxidant reduction on fuel surface (cathodic reactions on fuel surface)
- The rate of U(IV) → U(VI) oxidation (anodic reactions on fuel surface)
- The rate of H_2 production by steel corrosion and H_2 flux to the NMP sites on the fuel surface
- The rate of the oxidation of H_2 on the NMP catalytic sites (anodic reaction on fuel surface that anodically "protects" UO_2 from oxidation)

Since the rates of of H_2 generation on the steel and H_2 oxidation on the fuel play the dominant roles in determining the dissolution rate of the fuel, the on-going work on the FMDM has emphasized these processes.

Table 1. Summary of FMDM parameters and data gaps that need to be addressed in future work to improve the accuracy of the model.

Parameter	Description	Data needs to improve accuracy
Dimension of fuel environment	(mm – cm)	To be updated when dimensions of waste package are known
Nodes in fuel environment	(log-space grid: fine-spacing near surface)	To be updated when dimensions of waste package are known
Fuel surface coverage by NMP	(~1%)	From literature
Dimension of steel environment	(mm – cm)	To be updated when dimensions of waste package are known
Nodes in steel environment	(log-space grid: fine-spacing near surface)	To be updated when dimensions of waste package are known
Number of FMDM time steps	(100 – 1000)	Use to optimize PA interface
Fuel alteration layer porosity	(~50%)	From literature
Fuel alteration layer tortuosity	(~0.01)	From literature
Fuel alteration layer radiolysis factor	(*not used*)	*Could be activated to account for radionuclide uptake by U secondary phases*
Alpha particle penetration depth	(35μm)	From literature
Fuel burnup	(25 – 75 GWd/MTU)	Input from PA
Age of fuel (time out of reactor)	30 – 100 yrs	Input from PA
Resistance between fuel and NMP domains	(10^{-3} Volts/Amp)	Interpretation of literature
Temperature history	function	Data need: needs to be input from PA – will depend on repository scenario
Dose rate history	function	Based on MCNPX results of Radulescu, 2011
Spatial dose rate	function (decrease in dose rate with distance from fuel)	Based on MCNPX results of Radulescu, 2011
Rate constants for interfacial reactions in fuel and steel domains	See Figure 8 for summary of specific reactions	Data need: experiments needed due to lacking or inconsistent data in current literature on H_2 reactions on fuel and NMP and steel corrosion under relevant conditions
Charge transfer coefficients for interfacial half-cell reactions in fuel and steel domains	See Figure 8 for summary of specific reactions	Data need: experiments needed due to lacking or inconsistent data in current literature on H_2 reactions on fuel and NMP
Activation energies	T dependence: See Figure 8 for summary of specific reactions	Data need: experiments needed due to lacking or inconsistent data in current literature on H_2 reactions on fuel and NMP and steel corrosion under relevant conditions

Table 1. Continued.

Parameter	Description	Data needs to improve accuracy
Standard potentials for interfacial half-cell reactions: fuel and steel	See Fig. 8 for reactions	From literature
Relative area of fuel domain	Default 1:1, depends on waste package design	To be updated when dimensions of waste package are known
Relative area of steel domain	Default 1:1, depends on waste package design	To be updated when dimensions of waste package are known
Environmental leak rate (diffusion barrier factor)	Depends on waste package design, breach	Interpretation of literature
Environmental concentrations	(O_2, H_2, CO_3^{2-}, Fe^{2+}, Cl^-)	Input from PA
Rate constants for bulk solution reactions in fuel, steel environments	See Figure 6 for summary of specific reactions	From literature
Activation energy for bulk solution reactions	T dependence, See Figure 8 for reactions	From literature
Passivation potential of steel surface	(75 V_{SCE}) as place-holder	Data need: experiments needed due to lacking or inconsistent data in current literature
Passivation corrosion current density	Calculated internally within FMDM	Data need: experiments needed due to lack of data in literature
Radiolytic oxidant (H_2O_2) generation value (G_{cond})	Analytical function for conditional G_{H2O2} value from PNNL radiolysis model	Values based on radiolysis model results, Buck et al., 2013. *Would need to be updated, expanded for brine solutions (Cl, Br)*

The half-reactions for anoxic steel corrosion can be represented as:

$$Fe^0 \rightarrow Fe^{2+} + 2e^- \quad \text{(Reaction 1)}$$

$$2H_2O + 2e^- \rightarrow H_2 + 2OH^- \quad \text{(Reaction 2a)}$$
$$2H^+ + 2e^- \rightarrow H_2 \quad \text{(Reaction 2b)}$$

with the overall steel corrosion reaction

$$Fe + 2H_2O \rightarrow H_2 + Fe^{2+} + 2OH^- \quad \text{(Reaction 3a)}$$
$$Fe + 2H^+ \rightarrow H_2 + Fe^{2+} \quad \text{(Reaction 3b)}$$

Reactions 3b and 3a provide the fundamental coupling between steel corrosion and H_2 generation in acidic and neutral or alkaline solutions. (Analogous reactions can be written for Zircaloy corrosion to form ZrO_2.) The oxidation of other steel constituents (e.g., Cr, Mo, Ni, and Mn) will contribute to the anodic current but the oxidation of Fe is dominant. The threshold potential and reaction rate for Reaction 1 will depend on the surface potential imposed by the seepage water.

The conservation of charge requires that the sum of the current densities of all anodic and cathodic reactions in the system equals zero at equilibrium; this occurs at the corrosion potential (E_{corr}). That is, the corrosion potential represents the kinetic balance between anodic and cathodic reactions occurring in the system.

Since Reactions (1) and (2) are the dominant anodic and cathodic reactions on the steel surface, the rate of H_2 generation will equal the rate of Fe oxidation under anodic (oxidizing) conditions. The corrosion rates of different steels may vary significantly with their compositions, with the environmental conditions (primarily Eh, pH, and chloride concentration), and with the formation of passivating films. The corrosion rates can change significantly when the surfaces passivate to prevent water from contacting metallic iron. In the EBS, the Eh of the seepage water can impose surface potentials that are cathodic for some steels and anodic for other steels. Therefore, the FMDM must account for the corrosion behavior of each metal independently.

3. STEEL CORROSION MODULE

There are several advantages to the approach of incorporating a separate steel corrosion module directly into the FMDM as shown in Figures 8 and 10:

- It directly couples fuel degradation and steel corrosion. This is vital, as it has been shown that H_2 produced from the anoxic corrosion of steel can decrease the fuel dissolution rate by over four orders of magnitude (Jerden et al., 2015).
- Directly coupling the fuel and steel degradation kinetics allows for the quantification of redox fronts that develop within the waste container due to the diffusion of radiolytic oxidants away from the fuel surface and the reactions of these oxidants with the steel surface and the resulting aqueous Fe^{2+} and H_2. This is also important because these redox fronts represent the Eh of the seepage water contacting the waste form and waste container internal components.
- This approach will allow the steel corrosion module to be readily implemented into the GDSA PA model. The version of FMDM that has already been integrated with PA can be replaced with the new version that includes the steel corrosion module, since all changes occur within the FMDM. The only change to the PA interface will be including the Cl^- concentration of the groundwater.

The initial steel corrosion module used in the FMDM was adapted from King and Kolar, 2001 and is based on Butler-Volmer relationships between the corrosion currents and the surface potential. It consists of a simple mixed potential model with the reactions shown on the right side of Figure 8 and was implemented in the FMDM to evaluate the sensitivity of the calculated fuel degradation rates to steel corrosion rates. The module accounts for the transition between active and passive corrosion by defining a threshold potential ($E_{passive}$) above which the steel corrodes at a constant rate specified as the corrosion current density under passive conditions ($i_{passive}$). When the interfacial potential of the steel equals $E_{passive}$, the corrosion current density is assigned a maximum value ($i_{critical}$). If the solution Eh reaches higher potentials, the corrosion current density decreases to the passivation current density that is "hard-wired" in the module to represent constant corrosion of the passivated surface. This approach is simplistic, but provides "order of magnitude" differences sufficient to demonstrate the sensitivity of the fuel degradation rate. A more quantitative model is required to account for the dependencies on the environmental variables and surface stabilization to represent the combination of actively and passively corroding materials that will be present in the EBS. Section 6 describes the type of data needed to calibrate and parameterize a realistic electrochemical model.

The original steel corrosion mixed potential model formulated by King and Kolar, 2001 was based on the observation that carbon steel surfaces may undergo passive corrosion under alkaline conditions, due to the formation of a thin surface layer of Fe_3O_4 (Kaesche 1985, King and Kolar 2001, King, 2007). King, 2007 claims that carbon steel exposed to solutions that fall within the Eh – pH conditions corresponding to the magnetite stability field (e.g., Figure 9 above) will corrode passively. The critical anodic current density above which C-steel becomes passivated is ~1μA cm^{-2} at pH 9.5 (King and Kolar, 2001), which corresponds to a passivation potential of approximately -0.75 V vs SCE (-0.51 V vs SHE) (Kaesche 1985). However, other studies have shown that carbon steel does not passivate under the conditions expected in a crystalline rock repository with a bentonite buffer (JNC 2000). This discrepancy must be resolved for reliable modeling.

The model developed by King and Kolar, 2001 was only applied for C-steel. The FMDM steel model needs to account for not only C-steel, but also for other alloys in the spent fuel canisters, such as 316 stainless steel and borated stainless steels. The corrosion of Zircaloy cladding is another important source of H_2, but was not included in the FMDM sensitivity calculations.

Directly measuring the reaction current generated by the transfer of electrons during a redox reaction provides a sensitive and accurate measure of the reaction rate. The relationship between the cumulative charge transferred and dissolved mass is given by Faraday's Law:

$$m = \frac{QM}{nF} \qquad \text{Equation 1}$$

where m is the mass of substance oxidized, Q is the total electric charge passed through the electrode substance, M is the molecular weight of the electrode substance, F is the Faraday constant, and n is the number of electrons transferred.

The cumulative electric charge Q is the integrated reaction current measured at the electrode:

$$Q = \int_0^t I(t)\, dt \qquad \text{Equation 2}$$

where $I(t)$ is the reaction current measured at the electrode at time t. Therefore, the mass of material oxidized at the electrode surface can also be calculated from the measured reaction current at the electrode. If the corrosion current is constant, the mass corroded over an interval Δt can be calculated as:

$$m = \frac{I \cdot \Delta t\ M}{nF} \qquad \text{Equation 3}$$

and the rate can be calculated as

$$rate = \frac{m}{\Delta t} = \frac{I\,M}{n\,F}\,. \qquad \text{Equation 4}$$

The current and mass released can be normalized to the surface area of the electrode to give corrosion rates in units of g m^{-2} yr^{-1}, which can be converted to penetration rates in mm yr^{-1} using the density of the steel. It also gives the H_2 generation rate using the stoichiometry in Reaction 3.

The sensitivity study performed using the initial steel corrosion module in the FMDM, which is described in detail in Section 4 below, indicates that steel passivation has important implications for the rate of spent fuel degradation and the radionuclide source terms that are derived. An example of results from the sensitivity study is shown in Figure 11a for extreme cases of no steel corrosion and rates for passive corrosion (10 g m^{-2} yr^{-1}) and active corrosion (172 g m^{-2} yr^{-1}). Those steel corrosion rates are shown relative to the generic passivation model of King and Kolar in Figure 11b. (Details of the model runs discussed in Section 4).

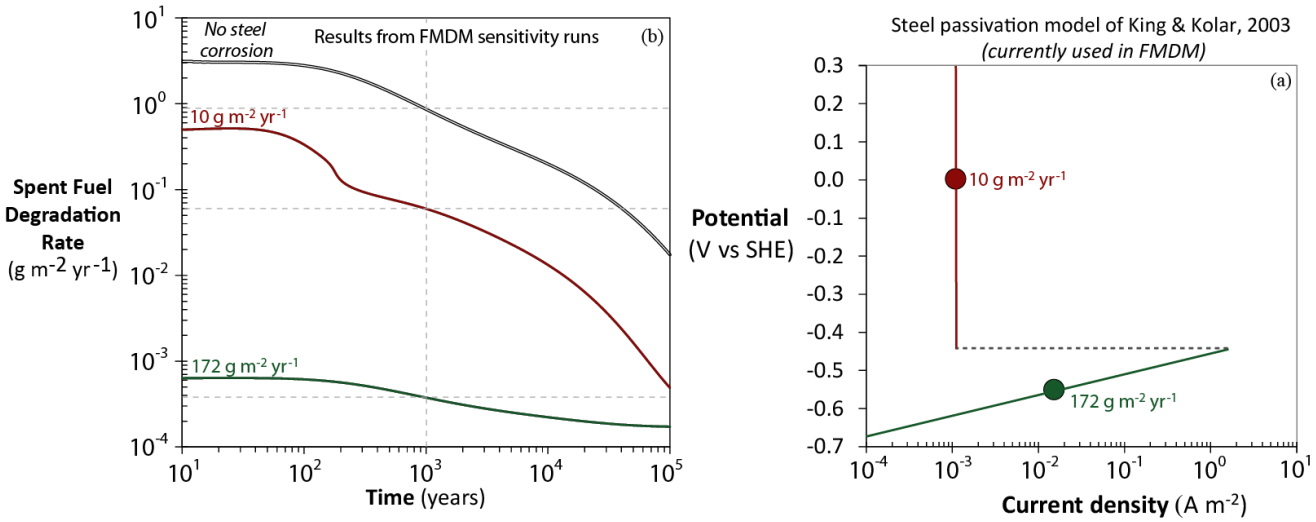

Figure 11. Examples of spent fuel degradation rates calculated for different steel corrosion rates (a). The higher steel corrosion rate of 172 g m^{-2} yr^{-1} represents active corrosion while the 10 g m^{-2} yr^{-1} value represents a passive corrosion rate (b).

Figure 11 shows that for the hypothetical case where steel within a failed canister corrodes at an active rate of 172 g m^{-2} yr^{-1}, the corresponding spent fuel degradation rate is about 0.0004 g m^{-2} yr^{-1} at 1000 years. This is more than 3 orders of magnitude lower than rate of 0.9 g m^{-2} yr^{-1} calculated for the no H_2 case (no steel corrosion). However, if the steel passivates under more oxidizing conditions and the steel corrosion rate decreases to 10.0 g m^{-2} yr^{-1}, the spent fuel degradation rate is predicted to be 0.06 g m^{-2} yr^{-1}, which is a factor of 150 higher than that predicted for active steel corrosion. This example highlights the importance of accurately modeling active and passive corrosion rates of different metals in a breached container as functions of Eh and other environmental variables. It also shows the need for a steel corrosion model more realistic than the initial model represented in Figure 11b to include those dependencies.

4. SENSITIVITY OF FUEL DEGREDATION RATE TO STEEL CORROSION

A series of model runs were done using the updated FMDM with the steel corrosion module over a range of relevant conditions. The purpose of these runs was to quantify the sensitivity of the FMDM-predicted fuel degradation rate to the rate of steel corrosion (despite the high uncertainties in the steel corrosion rates and ignoring environmental dependencies). The conditions for these sensitivity calculations are listed below and the model layout and examples of the results are shown in Figures 12 to 17.

- The variables that were changed for these sensitivity runs were the iron corrosion rate (Reaction 1) and the transport rate of dissolved species from the fuel – steel domain into the boundary domain (zero volume mixing cell on Figure 12).
    - The iron corrosion rate constant was varied to generate corrosion rates varying form 0.1 to 700 g $m^{-2}yr^{-1}$ (*actual values of this parameter need to be determined experimentally for relevant steel compositions and environmental dependencies*).
    - The diffusive transport rate of dissolved species (such as H_2) into the boundary domain was varied between 1×10^{-3} m^{-1} (open system) and 1×10^{-2} m^{-1} (closed system). The low

rate case (closed system) simulates a case where the transport of species is slowed by the presence of a diffusion barrier such as a mass of iron oxide corrosion products.

- Parameter values (see Table 1) for the fuel environment are from Jerden et al., 2015.
- Parameter values (see Table 1) for the steel environment are from King and Kolar, 2003 (the actual values of these parameters need to be determined experimentally for relevant types of steels).
- The environmental concentrations (constant concentration boundary) were $[H_2] = 1 \times 10^{-9}$ M, $[O_2] = 1 \times 10^{-9}$ M, $[Fe^{2+}] = 1 \times 10^{-9}$ M, $[CO_3^{2-}] = 1 \times 10^{-6}$ M.
- Temperature was held constant at 25 °C for all runs.
- The fuel burnup was 60 GWd/tHM (gigawatt days per metric ton of initial heavy metal: U).
- The age of the fuel for all model runs was 100 years old.

The model results indicate that the concentration of dissolved H_2 that reaches the fuel surface will vary considerably for the relevant range of steel corrosion rates. The variation in H_2 concentrations produced by this range of steel corrosion rates results in a range of H_2 concentrations from nanomolar to 0.1 millimolar, which causes the predicted fuel degradation rate to vary from 2×10^{-4} g $m^{-2}yr^{-1}$ up to 4.0 g $m^{-2}yr^{-1}$.

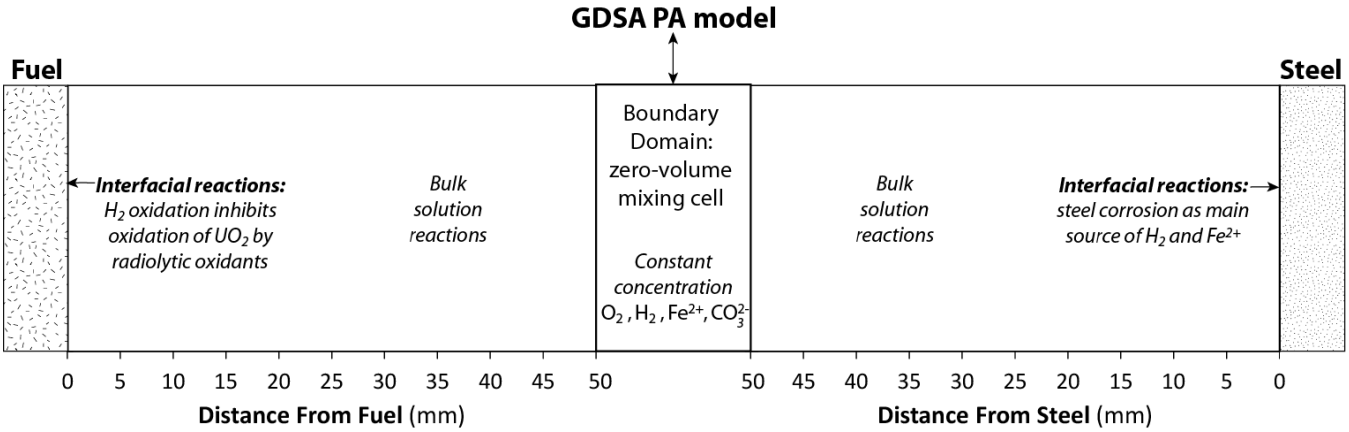

Figure 12. FMDM layout showing all domains and spatial relationships. See Figure 8 above for the details on the coupled reaction scheme.

Figure 13 shows the fuel degradation rates as a function of time coupled with a range of relevant steel corrosion rates for both open and closed system conditions. The rate of iron oxidation is equal to the rate of H_2 production at the steel surface. The fuel degradation rate decreases slowly as the dose rate at the fuel surface decreases due to the decreasing production rates of the radiolytic oxidant H_2O_2 and associated O_2 over time. As the amount of radiolytic H_2O_2 decreases, less H_2 is required to anodically protect the fuel from oxidative dissolution. The diffusion of radiolysis products from the fuel surface and H_2 from the steel surface to the boundary domain is not shown on the diagram. Both diffuse from the boundary domain to the other surface and, in the case of an open system, to outside the waste package through the breach.

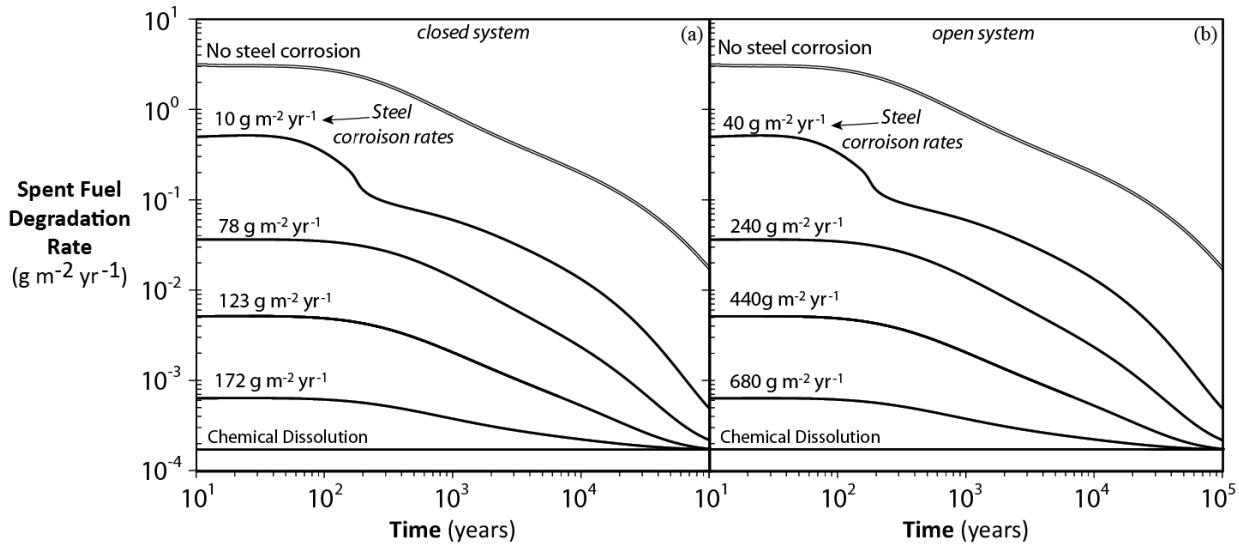

Figure 13. Results from the FMDM with the newly added steel corrosion module. The numbers shown for each curve are the steel corrosion rates, which are directly proportional to H_2 generation rates. All of these runs are for a 100 year old fuel with a burnup of 60 GWd/tHM. Diagram (a) is for a closed system case where the diffusive loss of dissolved species (such as H_2) to the boundary domain is relatively slow. Diagram (b) shows the steel corrosion rates needed to generate the same spent fuel degradation rate curves shown in (a) for an open system case where the leak rate is a factor of 10 higher than the closed system case.

Figure 13 demonstrates that for the closed system case (a), which simulates a scenario where the diffusion of aqueous species to the boundary domain are slowed by a diffusion barrier such as a mass of iron oxides, a steel corrosion rate of 172 g m^{-2} yr^{-1} maintains spent fuel degradation rates less than 10^{-3} g m^{-2} yr^{-1} . For the open system case [Figure 13 (b)] a steel corrosion rate of 680 g m^{-2} yr^{-1} is required to maintain fuel degradation rates less than 10^{-3} g m^{-2} yr^{-1}. This is because much of the H_2 that is generated escapes the system without contacting the fuel surface. Given that canister breaches will likely be filled with ferrous corrosion products and given the impervious nature of the surrounding bentonite buffer, the closed-system conditions are more likely.

Figure 14 shows two fuel degradation rate curves for the closed system case plotted with results from a number of spent fuel and UO_2 dissolution tests. The fuel tests were performed in oxidizing conditions using ~30 year old fuel that varied in burnup from 25 to 45 GWd/tHM [see Cunnane, 2004]. The temperatures for these tests varied from 25 °C to 80 °C, the pH varied from 7 to 9, and the solutions contained various concentrations of dissolved carbonate (zero to millimolar). The simfuel tests (Ollila, 2008) involved the immersion of ^{233}U doped UO_2 in buffered DIW at pH 7 – 9 and 25 °C to 90 °C; those tests were performed under anoxic conditions (argon purged) and reducing conditions (metallic iron added to tests). The modeled H_2 effect is consistent with the effects of the imposed Eh value and far exceeds the effects of variations in the environmental conditions.

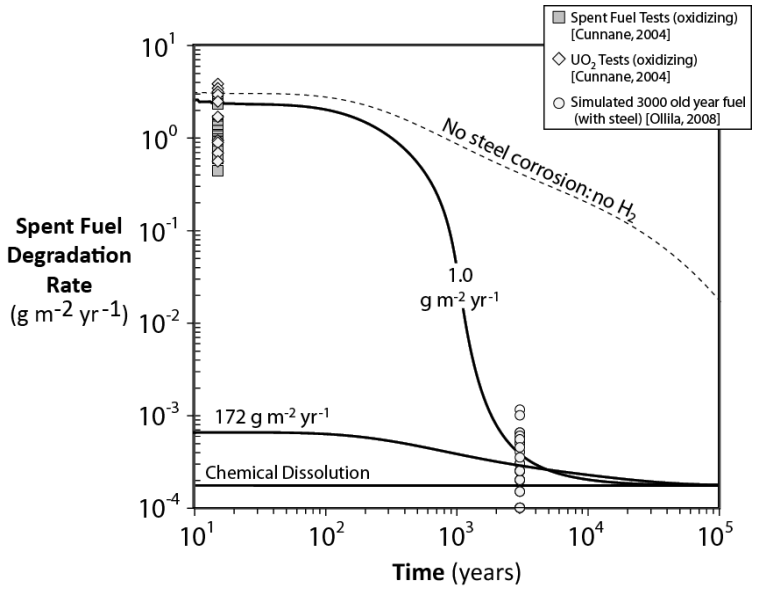

Figure 14. Results from the FMDM with and without the steel corrosion module and data from selected spent fuel and UO_2 dissolution tests. The numbers shown for each curve are the steel corrosion rates, which are directly proportional to H_2 generation rates. Both runs are for a 100 year old fuel with a burnup of 60 GWd/tHM.

The sudden decrease in fuel degradation rates in the 1.0 g $m^{-2}yr^{-1}$ curve in Figure 14 is attributed to the accumulation of H_2 within the porous U(VI) alteration phase layer, which is shown schematically at the bottom of Figure 8. As will be demonstrated below, aqueous species accumulate within the pores of the U(VI) layer because their diffusion is slowed by a tortuosity factor. This allows H_2, which rapidly diffuses from the steel surface to the fuel surface, to accumulate to a relatively high concentration near the fuel surface. A similar sudden decrease in the fuel degradation rate is not seen in Figure 14 when the steel corrodes at 172 g $m^{-2}yr^{-1}$ because an alteration layer does not form. The fuel degradation rate is low enough under those conditions that solution never becomes saturated with respect to schoepite, which is the primary mineral in the U(VI) alteration layer.

The effect that H_2 accumulation in the U(VI) alteration layer has on spent fuel degradation rates is further illustrated in Figures 15, 16, and 17 to show the effects of other model parameters. Figure 15 shows fuel dissolution rate curves for no steel corrosion and for a steel corrosion rate of 2.0 g $m^{-2}yr^{-1}$ under closed system conditions with tortuosity factors of 0.1 (the default value) and 0.9 representing the porosity of the U(VI) alteration layer. The higher tortuosity factor (0.1) leads to slower diffusion in the alteration layer and greater accumulation of H_2 resulting in a sudden decrease in fuel degradation rate. The decrease is more gradual in the lower tortuosity factor (0.9) case. The H_2 dissolved concentration profiles for the 0.1 tortuosity factor case are shown in Figure 16. The zero-volume mixing cell is located 50 mm from the fuel and steel surfaces. The H_2 concentration profile in the steel domain (right panel in Figure 16) is constant with time because it represents a steady state between the constant rate of H_2 production at the steel surface and the constant rate of loss to the environment at the 50 mm point. Diffusion from the steel surface fixes the H_2 concentration at a distance of 50 mm from the fuel surface. The H_2 concentration profile in the left panel of Figure 16 varies with time in the fuel domain because the rate of consumption of H_2 at the fuel surface decreases with time. This decrease corresponds to the decrease in the corrosion potential of the fuel due to the decrease in radioytic oxidant production.

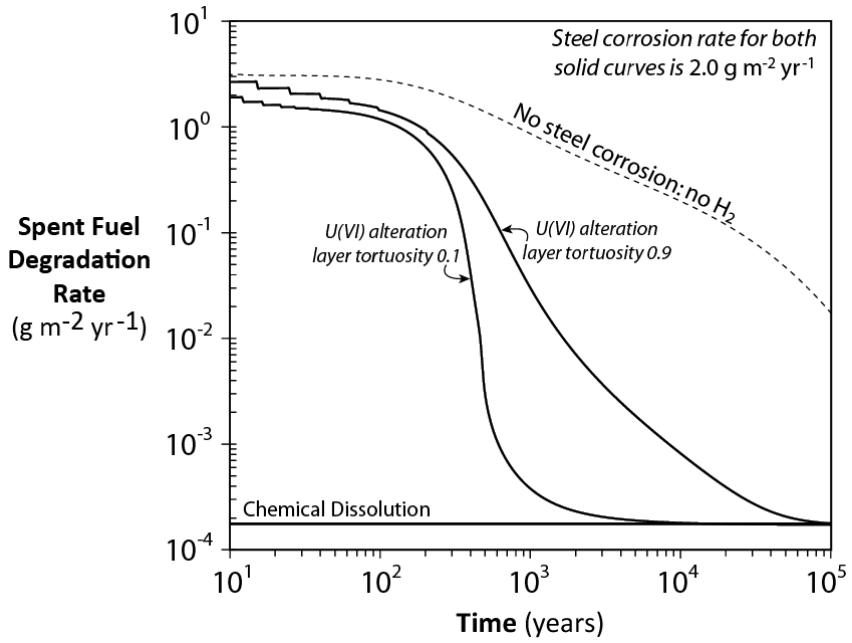

Figure 15. Results from the FMDM with the steel corrosion module. The two curves, both for a steel corrosion rate of 2.0 g $m^{-2}yr^{-1}$ are for different tortuosity values applied to the U(VI) alteration layer. The tortuosity value is applied as a factor that slows diffusion, allowing a buildup of species within the porous layer.

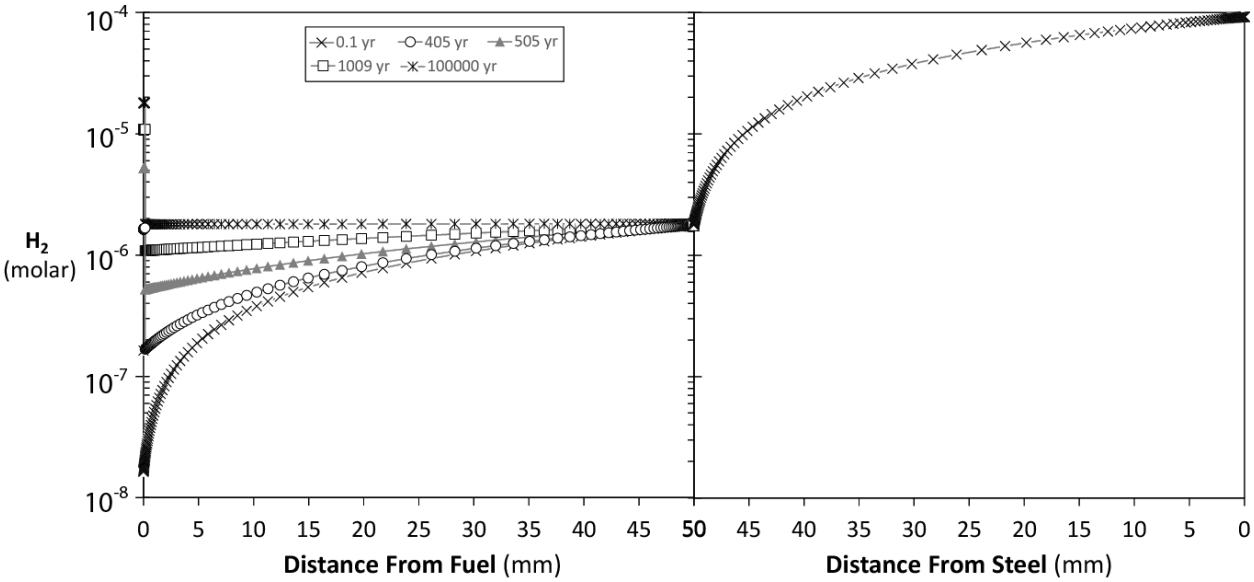

Figure 16. Dissolved concentrations of H_2 within the FMDM reaction diffusion cell for the 2.0 g $m^{-2}yr^{-1}$ steel corrosion curve with a U(VI) layer tortuosity factor of 0.1. The reason for the discontinuity at 50 mm is that H_2 is lost to the environment (through zero volume boundary domain) at that location (see Figure 12).

Figure 17 shows the concentration profiles for H_2 within the first 300 micometers of the fuel surface for the same case as Figure 16 (2.0 g $m^{-2}yr^{-1}$ steel corrosion rate, closed system conditions, tortuosity factor of 0.1). Figure 17 illustrates the accumulation of H_2 in the alteration layer and at the fuel surface that occurs in the

model. The thickness of the alteration layer increases with time, but reaches a maximum thickness of 130 μm after 307 years.

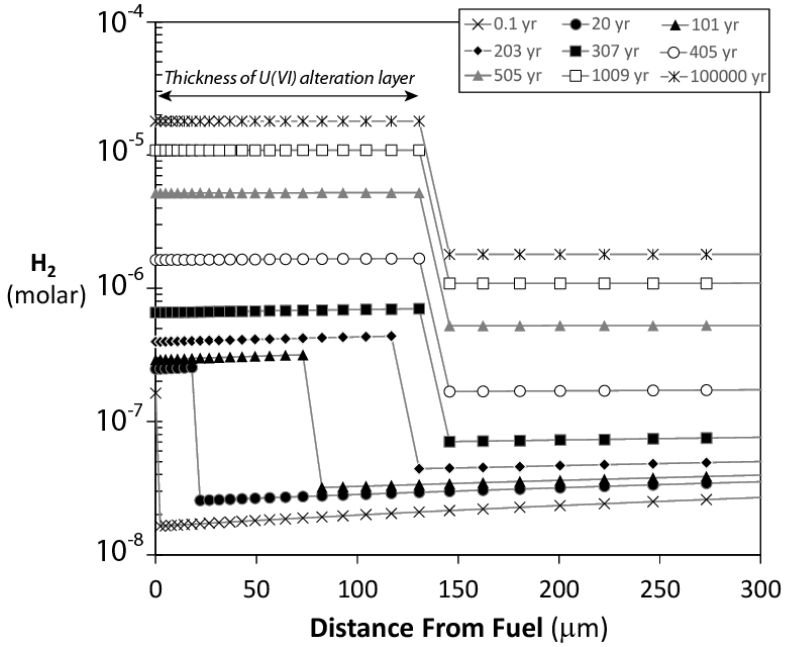

Figure 17. Dissolved concentrations of H_2 within the FMDM reaction diffusion cell for a steel corrosion rate of 2.0 g $m^{-2}yr^{-1}$. The discontinuity in each profile identifies the thickness of the alteration layer, which reaches a maximum value of 135 μm after 307 years.

5. EXAMPLE IN-PACKAGE CHEMISTRY SIMULATION: STEEL TITRATION MODEL

To investigate how the H_2 concentration within a failed canister may evolve as the spent fuel and various types of steels corrode simultaneously, a simple titration model was developed and run in the thermodynamic code: Gechemist's Workbench (Bethke, 2014). The thermodynamic database used for this model was thermo.com.V8.R6 (Johnson et al, 2000) to which the steel reactants were added. The masses of the different steel components and total solution volume were taken from the in-package chemistry model used for the YM TSPA (CRWMS, 2003). The masses used for this model are shown in Table 2, the compositions of the materials are shown in Table 3 and the initial groundwater composition, which is typical of a crystalline rock repository environment, is shown in Table 4. The initial volume of solution used in the model was 4.1 m^3, which is based on the void volume within the spent fuel canister assumed in CRWMS, 2003.

Table 2. Values used in the Geochemist's Workbench steel titration model (from CRWMS, 2003).

Materials	**Total Mass** (kg)	**Specific Surface Area** (m^2 g^{-1})	**Total Area** (m^2)
316 SS	$5.9x10^3$	$4.1x10^{-6}$	24.2
Borated SS	$1.2x10^3$	$4.5x10^{-5}$	52.9
C-steel: A516	$2.1x10^3$	$8.7x10^{-5}$	180.5

Table 3. Compositions of steels used in Geochemist's Workbench steel titration model (from CRWMS, 2003).

Component	**316 SS**	**Borated SS** (Neutronit)	**C-steel: A516**
C	0.02	0.04	0.28
Mn	2.0	---	1.05
P	0.05	---	0.04
S	0.03	---	0.04
Si	0.75	---	0.29
Cr	17.0	18.5	---
Ni	12.0	13.0	---
Co	---	0.2	---
Mo	2.5	2.2	---
N	0.08	---	---
Fe	65.58	64.82	98.3
B	---	1.25	---

Table 4. Initial solution composition used in Geochemist's Workbench steel titration model (from Posiva, 2012). This composition is typical of groundwaters in a crystalline rock repository environment.

Component	Concentration (molar)
pH	8.2
Na	0.36
Ca	0.25
K	4.9×10^{-4}
Mg	1.5×10^{-3}
Sr	1.1×10^{-3}
Mn	9.3×10^{-6}
Fe	3.8×10^{-7}
Cl^-	0.86
SO_4^{2-}	2.1×10^{-4}
CO_3^{3-}	4.0×10^{-5}
SiO_2	2.1×10^{-4}

Results from two separate model scenarios using high and low steel corrosion rates are presented below. The first involved the titration of materials described in Tables 2 and 3 into the solution shown in Table 4 using the following constant rates:

- C-steel: 172 g m^{-2} yr^{-1}
- 316 SS: 85 g m^{-2} yr^{-1}
- Borated SS: 85 g m^{-2} yr^{-1}.

The same rates were used for 316 SS and borated SS, but the masses and compositions are different. Two different cases were run for this scenario, one in which the solution contained 10 mM dissolved O_2 at the beginning of the run [Figure 18(a) and 18(c)] and another where the initial dissolved O_2 was 1 μM at the start of the simulation [Figure 18(b) and 18(d)]. As shown in Figure 18, evolution of the solution pH and Eh is strongly influenced by the initial O_2 concentration. Under initial oxidizing conditions, the pH of the solution decreases from a starting value of 8.2 down to near 5.0, but increases to 9 once the O_2 is depleted. The early pH decrease is not observed with low starting O_2 (Figure 18b).

The initial Eh conditions predicted in the Geochemist's Workbench steel titration model for the high O_2 scenario fall within the U(VI) and ferric oxide stability fields (see Eh – pH diagrams in Figures 2 and 9 above). However, once the O_2 is consumed, the solution becomes reducing with respect to the U^{4+}/U^{6+} and Fe^{2+}/Fe^{3+} couples. The only source of oxidants within this reducing in-package solution is H_2O_2 and associated O_2 formed by radiolysis near the spent fuel.

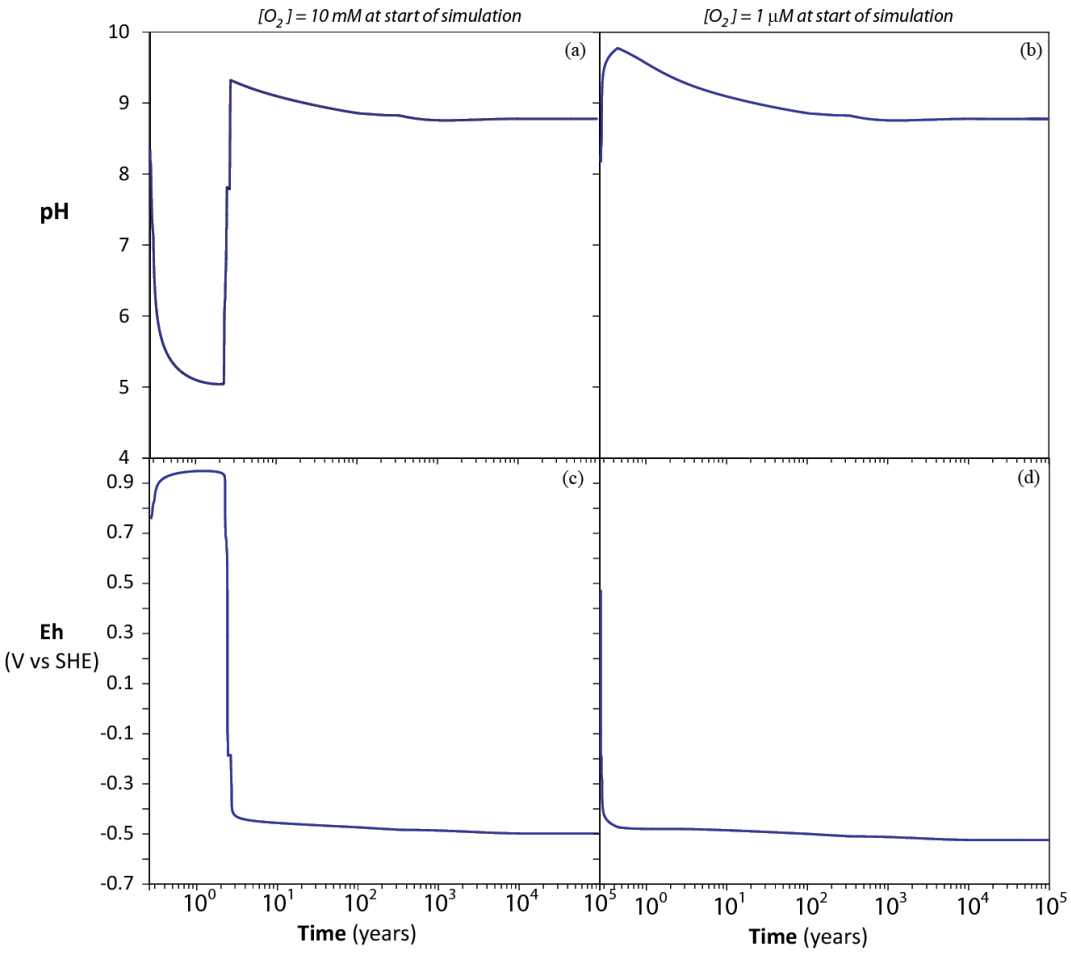

Figure 18. Results from the Geochemist's Workbench steel titration model using the materials described in Tables 2 – 4.

The pH evolution shown for the results shown in Figure 18 are likely the result of the Reactions (1) – (9). The early pH decrease in the 10 mM O_2 case is likely caused by the oxidation of zero valent elements in the steel [reactions (1) and (3)], while the pH increase with time is likely due to the H^+ consuming reduction reactions (4) and (6). Note that the net H^+ production/consumption during the formation of hematite and magnetite is zero based on Reactions (9) – (11).

$S + H_2O + 1.5\ O_2(aq) \leftrightarrow 2\ H^+ + SO_4^{2-}$ (Reaction 3)

$C + H_2O + O_2(aq) \leftrightarrow H^+ + HCO_3^-$ (Reaction 4)

$P + 1.5\ H_2O + 1.25\ O_2(aq) \leftrightarrow 2\ H^+ + HPO_4^{2-}$ (Reaction 5)

H^+ consumption reactions:

$SO_4^{2-} + H^+ \leftrightarrow HS^- + 2\ O_2(aq)$ (Reaction 6)

$SO_4^{2-} + 2\ H^+ \leftrightarrow H_2S(aq) + 2\ O_2(aq)$ (Reaction 7)

$HCO_3^- + H^+ + H_2O \leftrightarrow CH_4 + 2\ O_2(aq)$ (Reaction 8)

Iron oxide formation reactions:

$Fe^0 + 2\ H^+ + 0.5\ O_2(aq) \leftrightarrow Fe^{2+} + H_2O$ (Reaction 9)

$3\ Fe^{2+} + 3\ H_2O + 0.5\ O_2(aq) \leftrightarrow Fe_3O_4 + 6\ H^+$ (Reaction 10)

$2\ Fe^{2+} + 2\ H_2O + 0.5\ O_2(aq) \leftrightarrow Fe_3O_4 + 6\ H^+$ (Reaction 11)

Figure 19 shows how the masses of solids change over time for the same model scenario shown Figures 18(a) and 18(c) (10 mM initial O_2). At the steel corrosion rates given above, the model predicts that all of the C-steel and borated steel in the package will be consumed after approximately 2000 years and all of the 316 stainless steel will be consumed after around 25,000 years. The primary iron oxide phases are ferric oxides and oxyhyroxides within the first few years of the simulation, but magnetite becomes the dominant oxide phase once the initial O_2 is depleted and will likely represent the main alteration phase formed on C-steel. Trevorite and chromite are predicted to form on the 316 SS and borated SS. Although it is not predicted in the simulations, Cr_2O_3 will form to passivate the 316 steels.

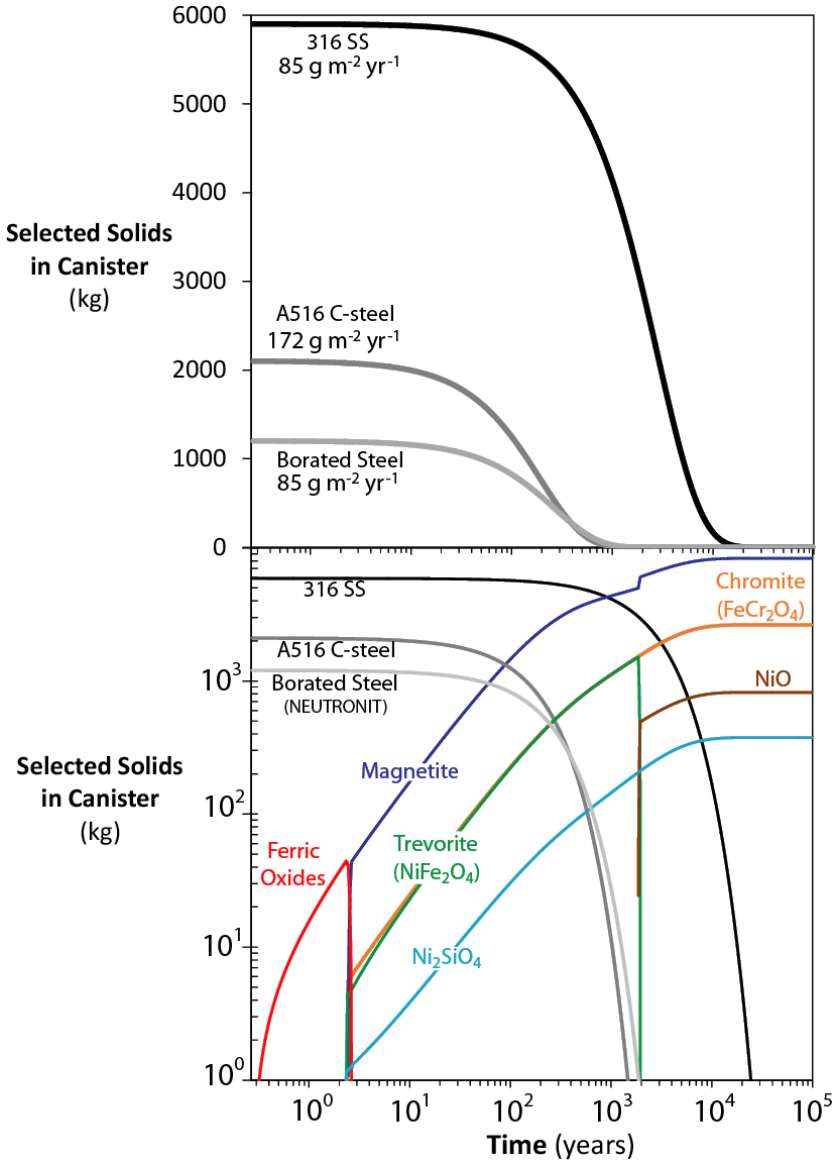

Figure 19. Results from the Geochemist's Workbench steel titration model using the materials described in Tables 2 – 4.

The impacts that the steel consumption rates calculated for the model scenario shown in Figure 19 have on spent fuel degradation are shown in Figure 20. In these FMDM runs, the overall H_2 generation rate was determined by the steel corrosion rates. The steel consumption rates determined how the fuel degradation rate changed as the different types of steels were consumed.

The FMDM results for the closed system case [Figure 20 (a)] show that the spent fuel dissolution rate is very similar to the rate of UO_2 chemical dissolution as long as some C-steel remains. This indicates there is enough H_2 being generated to inhibit oxidative dissolution of the fuel. However, when the C-steel is consumed after about 1000 years, the fuel dissolution rate increases to > 0.01 g m^{-2} yr^{-1}, due to the smaller amounts of H_2 generated by corrosion of the remaining 316 SS and borated SS. This is still a factor of 100 below what the degradation rate would be in the absence of H_2. The calculated fuel degradation rate increases to the oxidative dissolution rate when the 316 SS and borated SS are completely consumed after about 2000 years and H_2 is no longer being generated. The same trends are observed in the open system case [Figure 20 (b)], but the fuel dissolution rates are higher even with C-steel is present because a relatively large amount of H_2 is escaping the waste package into the environment and not reaching the fuel surface.

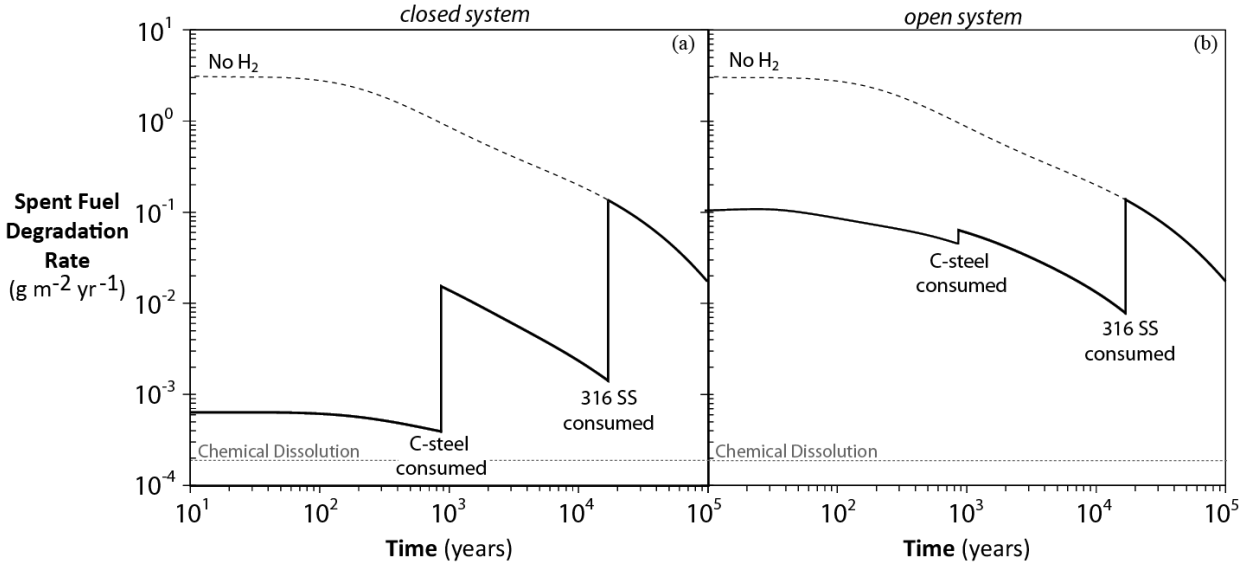

Figure 20. Results from the FMDM runs using the results from the Geochemist's Workbench steel titration model (Figures 18 and 19).

Results from a second Geochemist's Workbench model scenario with lower steel corrosion rates are shown in Figures 21, 22 and 23. This second scenario involved the titration of the same materials described in Tables 2 and 3 into the solution shown in Table 4 using the following constant rates:

- C-steel: 18 g m^{-2} yr^{-1}
- 316 SS: 1 g m^{-2} yr^{-1}
- Borated SS: 1 g m^{-2} yr^{-1}

Two different cases were run for this scenario, one in which the solution contained 10 mM dissolved O_2 at the beginning of the run [Figure 21(a) and 21(c)] and another where the initial dissolved O_2 was 1 μM at the start of the simulation [Figure 21(b) and 21(d)]. As shown in Figure 21, evolution of the solution pH and Eh are strongly influenced by the initial O_2 concentration. Under initial oxidizing conditions the pH of

the solution decreases from a starting value of 8.2 down to 4.5 before increasing up to > 9 once the O_2 is depleted. The early pH decrease is not observed with low starting O_2 (Figure 21b). The lower steel corrosion rates lead to a longer time interval in which the in-package solution is relatively acidic [~30 years in Figure 21(a) vs ~2 years in Figure 18(a)]. This is due to the lower rate of O_2 consumption for the slower steel corrosion case.

As with the first scenario described above, the initial Eh conditions predicted in this model fall within the U(VI) and ferric oxide stability fields (see Eh – pH diagrams in Figures 2 and 9 above); however, once the O_2 is consumed, the solution becomes reducing with respect to the U^{4+}/U^{6+} and Fe^{2+}/Fe^{3+} couples. Again, the only source of oxidants within this reducing in-package solution is H_2O_2 and associated O_2 formed by radiolysis near the spent fuel.

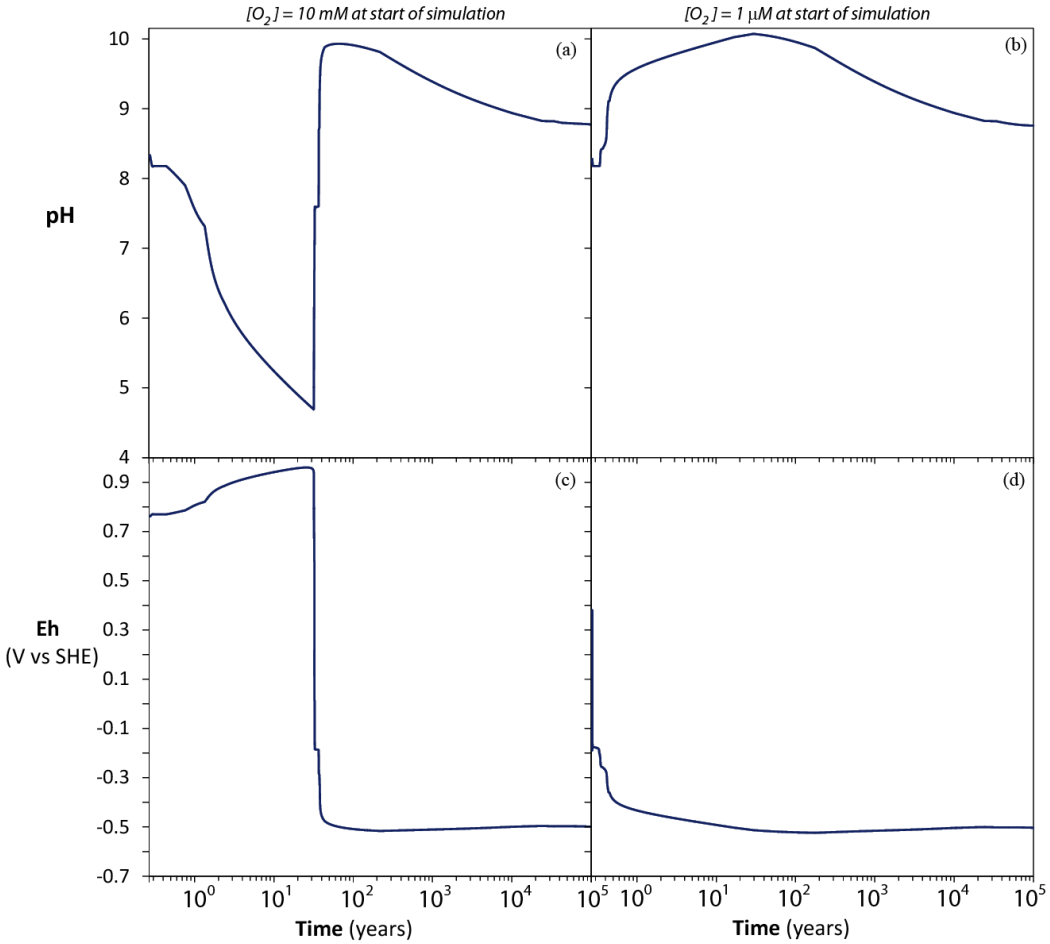

Figure 21. Results from the Geochemist's Workbench steel titration model using the materials described in Tables 2 – 4.

Figure 22 shows how the masses of solids change with time for the conditions shown in Figures 21(a) and 21(c) (10 mM initial O_2). The model predicts that all of the C-steel and borated steel in the package will be consumed after approximately 15,000 years at the lower steel corrosion rates, while the 316 SS persists for the entire 100,000 year simulation time. The primary iron oxide phases predicted to form within the

first few years of the simulation are ferric oxides and or oxyhyroxides, but magnetite becomes the dominant oxide phase once the O_2 is depleted and will likely represent the main corrosion product of C-steel, while chromite and nickel silicates and oxides will likely form on the 316 SS. Although it is not predicted in the simulations, Cr_2O_3 will form to passivate the 316 steels.

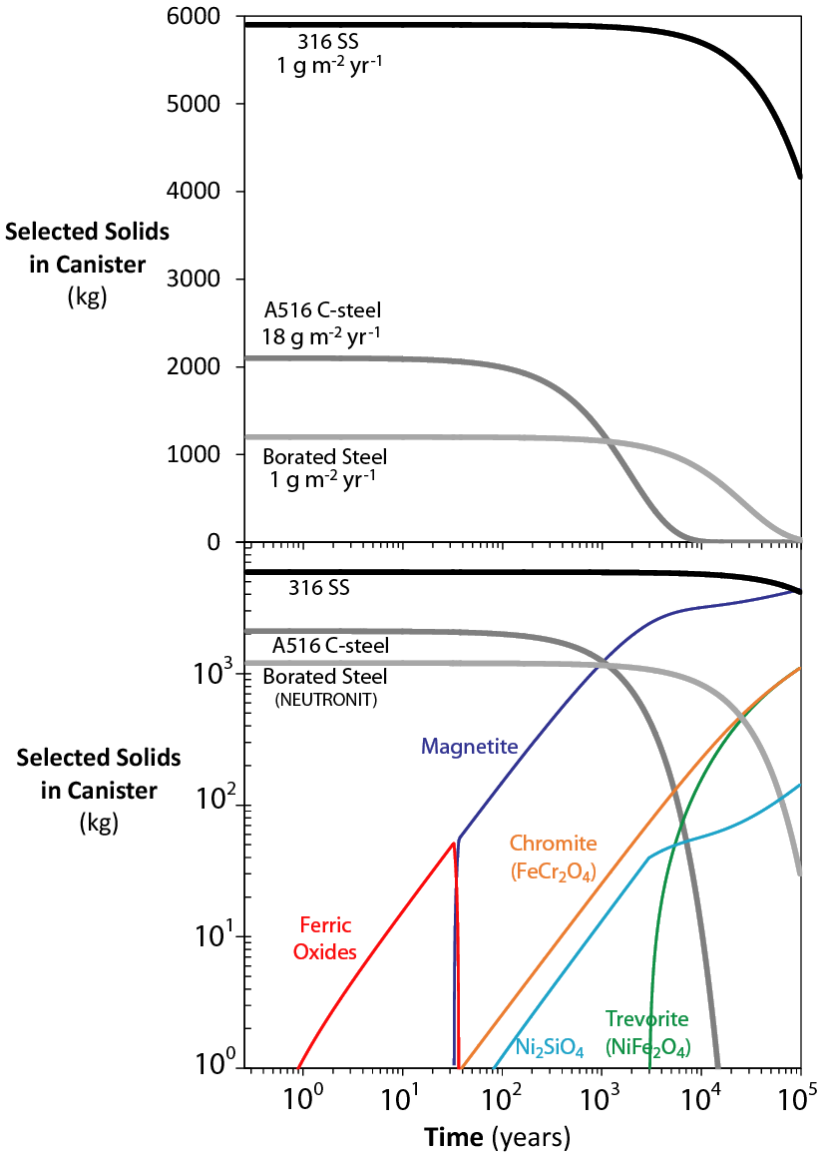

Figure 22. Results from the Geochemist's Workbench steel titration model using the materials described in Tables 2 – 4.

The impacts that the steel consumption rates from the model scenario shown in Figure 22 have on spent fuel degradation are shown in Figure 23. For these FMDM runs, the steel consumption rates from the Geochemist's Workbench model were used to predict how the fuel degradation rate changes when the different types of steels are consumed and the H_2 generation rates (equivalent to steel corrosion rates) change.

The FMDM results for the closed system case [Figure 23 (a)] show that the spent fuel degradation rate remains around 30 times lower than for the case with no H_2 (dotted line) for as long as C-steel remains. When the C-steel is completely consumed, the fuel degradation rate increases by approximately a factor of 10, but remains below the rate when no H_2 is generated due to the continued corrosion of 316 SS and borated steel. For the open system case [Figure 23 (b)], a dramatic decrease in the fuel degradation rate is predicted after about 100 years due to the accumulation of H_2 within the porous U(VI) alteration layer that forms under the oxidizing conditions that prevail early in the modelled scenario. The build-up of H_2 within the U(VI) layer is described in Section 4 above (see Figures 15 to 17).

It is unknown whether the H_2 accumulation process responsible for the sharp drop in fuel degradation rates shown in Figure 23(b) and in Figures 15 to 17 above is a real phenomenon or an artifact of how the system is modeled. This is clearly a significant uncertainty that must be clarified using carefully controlled experimental techniques to quantify and distinguish surface properties and diffusion processes.

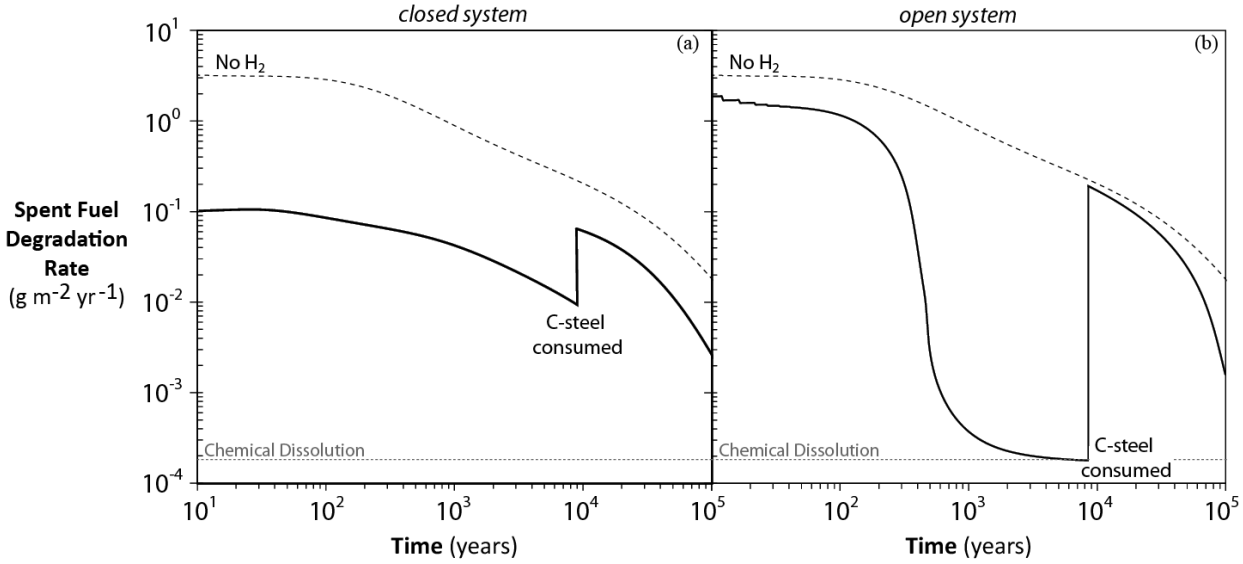

Figure 23. Results from the FMDM runs using the results from the Geochemist's Workbench steel titration model (see Figures 21 and 22 above).

Steel coupon immersion tests provide useful information on mineralogy and the evolution of the chemical system, but the Eh, pH and solution chemistry are not controlled during those tests and the surface conditions can change significantly during tests with passivating materials. Johnson and King, 2003, compiled a number of data sets with C-steel corrosion rates from coupon tests performed under conditions anticipated in crystalline rock repository setting with a bentonite buffer material. The corrosion rates from various coupon tests are summarized in Figure 24 and range from 0.1 g m^{-2} yr^{-1} to 1200 g m^{-2} yr^{-1}.

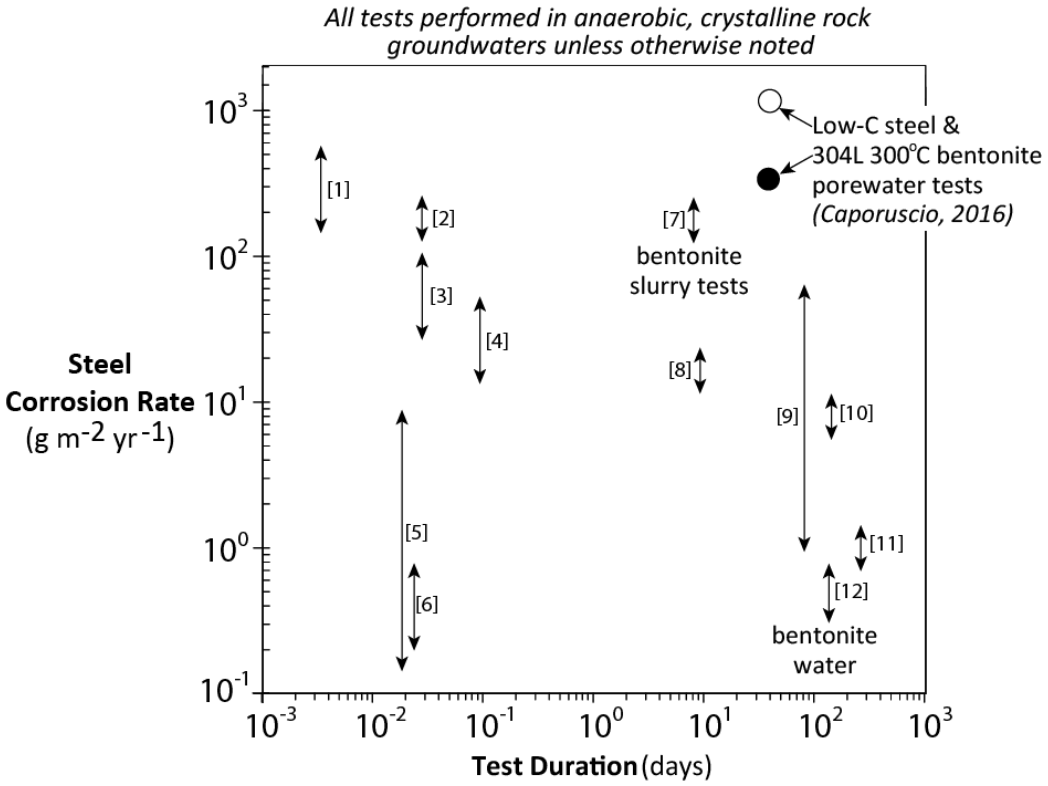

Figure 24. C-steel corrosion rates in groundwaters typical of crystalline rock repository environments and bentonite buffer materials (adapted from Johnson and King, 2003). [1] Simpson and Valloton (1986), [2] Lanza and Ronseco (1986), [3] Simpson and Valloton (1986), [4] JNC (2000), [5] DeBruyn et al. (1991), [6] Marsh and Taylor (1988), [7] Simpson (1989), [8] Simpson (1989), [9] Miller et al. (1994), [10] Smart et al., (2001), [11] Peat et al. (2001), [12] Smart et al. (2001).

The wide range of measured rates indicates coupon tests do not provide sufficiently accurate steel corrosion rates. Corrosion rates derived from mass loss are average cumulative values for the test duration that do not represent the effects of passivation that occurs within the first few days and can decrease the corrosion rate by several orders of magnitude. The difference between the cumulative rates from immersion tests and instantaneous rates measured with electrochemical methods is illustrated in Figure 25, where the green curve shows hypothetical mass loss as corrosion occurs during a coupon corrosion test. At the end of the test duration, the corroded material is removed from coupon to measure the mass loss and determine the average corrosion rate. The majority of mass loss that occurred prior to passive stabilization dominates the cumulative mass loss and the average rate. However, the instantaneous (kinetic) rate that is given by the slope of the curve decreases significantly as the surface stabilizes and becomes much lower than the average cumulative rate. The instantaneous rate that is measured directly as the corrosion current with electrochemical methods is needed to calculate the H_2 generation rate in the FMDM, not the average rate of the cumulative mass loss.

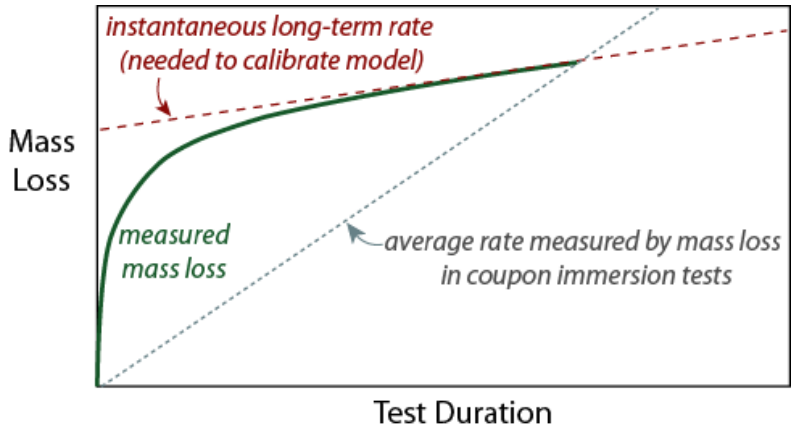

Figure 25. Conceptual diagram showing how mass loss measurements of steel corrosion rates yield rates that are significantly higher than the instantaneous rates relevant for repository process modeling.

Electrochemical tests provide corrosion rates under controlled environmental conditions and quantify the effects of surface stabilization due to passivation and localized corrosion, such a pitting, that can only be approximated in coupon immersion tests. Furthermore, electrochemical methods can measure rates on the order of nanograms cm^{-2} d^{-1}. The use of electrochemical methods would provide reliable corrosion rates for durable EBS materials (including Zircaloy cladding) and provide dependencies on environmental conditions that could be used to predict the long-term generation of H_2 and attenuation of fuel degradation rates as the seepage water composition evolves.

For example, Figure 26a shows the polarization curves measured for a carbon steel, a stainless steel, and Zircaloy-4 in a pH 4 solution using the ANL method as part of the DOE Nuclear Energy University Program project DE-NE-IL-UIC-0203-02 (Ebert 2017). These materials show different corrosion behaviors: carbon steel corrodes actively at very low potentials and does not passivate; stainless steel and Zircaloy-4 are noble at potentials below about -0.2 V; 316L passivates at moderate potentials, but corrodes actively above about 0.5 V; Zircaloy-4 passivates to high potentials in the absence of chloride (as shown), but passivation breaks down in the presence of even small amounts of chloride. (Note the difference in these profiles with that represented in Figure 11b.) Figure 26b shows the corrosion currents measured in potentiostatic tests conducted with these materials at potentials slightly above the E_{corr} values. The corrosion currents in tests with Zircaloy-4 and 316L decrease as the surfaces are rapidly passivated in the pH 4 solution. Relative to the currents measured for the freshly polished clean surfaces in the potentiodynamic scans, the corrosion currents decrease about 1.5 and three orders of magnitude due to passivation of Zircaloy-4 and 316L, respectively. The initial corrosion rate of 316 SS is 630 g m^{-2} yr^{-1} (measured in the PD scan) but the steady state rate of the stabilized surface appropriate for calculating H_2 generation in the FMDM is only 1.4 g m^{-2} yr^{-1}. This is represented qualitatively in the model of King and Kolar, but a more quantitative model is needed for reliable calculations in the FMDM.

The corrosion currents measured for the stabilized surfaces are appropriate for modeling the long-term H_2 generation rates in the FMDM; the currents measured in the potentiodynamic scans are not. Note that the low passivated rates for Zircaloy-4 and 316L were readily measured electrochemically, but these could not have been measured by mass loss in coupon immersion tests. The corrosion behaviors and rates will be different under different environmental conditions, and the differences must be taken into account in the FMDM. The electrochemical method developed at ANL (Ebert and Gattu 2016, Ebert et al. 2017) can be used to (1) measure corrosion rates for stabilized surfaces under controlled environmental conditions, (2) characterize the electrical properties of the passivated surfaces to provide confidence in their long-term stability, and (3) derive analytical expressions for key dependencies (Eh, pH, T, chloride concentration) that are required to calculate H_2 generation rates in the FMDM.

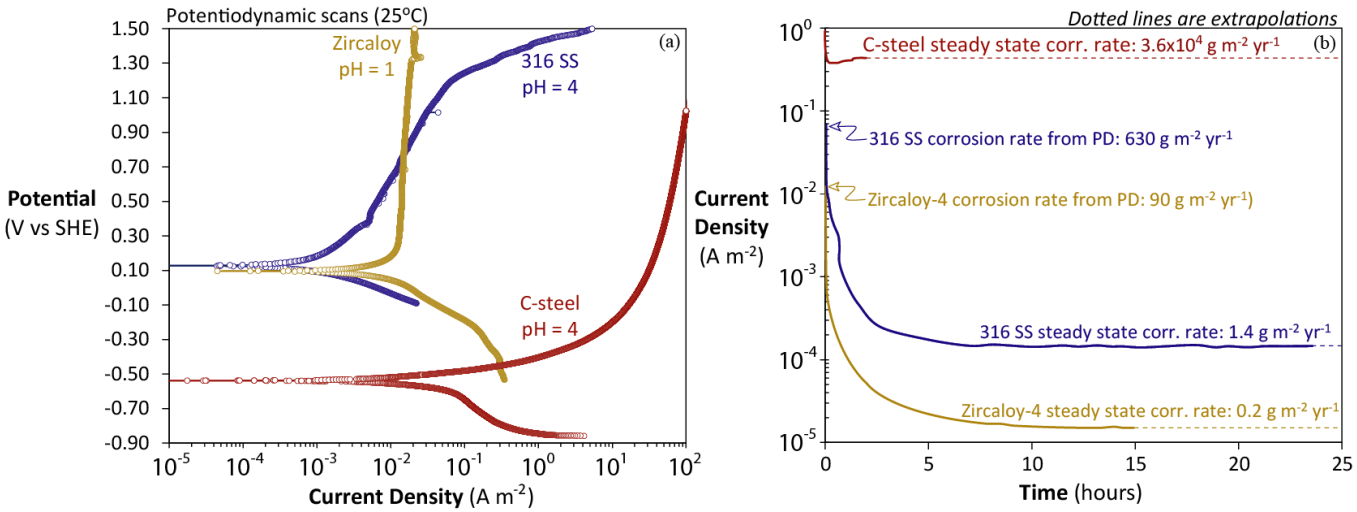

Figure 26. Results of electrochemical measurements at ANL for (a) potentiodynamic polarization and (b) potentiostatic corrosion of carbon steel at -0.4 V and pH = 4, 316L stainless steel at 0.5 V and pH = 4, and Zircaloy-4 at 0.5 V in pH 1 solution. The current densities measured in the PD scans are shown in (b) to illustrate the extents of passive stabilization for 316 SS and Zircaloy-4.

6. RECOMMENDATIONS

A number of information gaps were identified for modeling the anoxic corrosion behavior of relevant steels in repository-relevant conditions and the impact on spent fuel degradation rates. The magnitudes of the impacts of these processes were summarized in Figure 13, which showed fuel degradation rate curves for the cases in which no H_2 is generated (dotted line), for steel corrosion rates of 2 and 172 g m^{-2} yr^{-1}, and for the chemical dissolution rate. The high priority needs are summarized in Table 5.

Table 5. Information gaps identified as part of the present work.

Process	Issue and Data Needed	Experimental Approach
Long-term steel corrosion and H_2 generation rates at controlled Eh, pH, and and Cl^-.	Wide ranges of steel corrosion rates have been measured from mass loss in coupon tests under poorly controlled conditions; Those tests provide average rates that do not distinguish rates before and after passivation. Instantaneous steel corrosion rates with environmental dependencies (Eh, pH, Cl^-, T) are needed to calibrate and validate the fuel matrix degradation model.	Electrochemical measurements of steel corrosion rates and dependencies on T, Eh, pH, and Cl^- conditions after passivation.
Dissolution rates of aged, high burn-up fuels in the presence H_2 from steel corrosion	Based on canister design characteristics, it is likely that much of the spent fuel in the repository will not be exposed to groundwater until > 1000 yr after repository closure. More studies are needed on the dissolution rates of actinide oxide materials that simulate "aged" ~1000 yr old fuel in the presence and absence of H_2.	Synthesis of fission product and actinide doped simfuel, electrochemical measurements in the presence and absence of corroding steels
The roles that the porous corrosion layers (formed on the fuel and steel) play in the kinetics of spent fuel matrix degradation	Sensitivity runs performed with the FMDM (presented above) indicate that the presence of a porous corrosion layer on the fuel surface will facilitate accumulation of oxidants and reductants (most importantly H_2) at the fuel/solution interface to enhance the attenuating effect. This process has not been confirmed or quantified experimentally.	Generation of corrosion product layers on fuel simulant and steels under controlled conditions (potentiostatic), corrosion rate measurements under controlled conditions with and without corrosion product layer coupled with solution analyses and microscopy.

Due the high sensitivity of the fuel degradation rate to steel corrosion rates, it is recommended that the initial steel corrosion rate model be revised to include dependencies on environmental variables . Corrosion rates of likely EBS materials should be measured under the anticipated range of relevant conditions to derive analytical functions for key variables (Eh, pH, T, Cl^- concentration) that can be used in the FMDM. The scenario that needs to be studied involves post canister breaching conditions when the temperature will likely be 40 ^oC or lower (beyond 1000 years) with an initial solution composition similar to that shown in Table 4. The sensitivity of steel corrosion kinetics to environmental conditions is complex and should be represented as accurately as possible in the FMDM.

7. CONCLUSIONS

The objective of this study was to develop and test a process model for the degradation of uranium oxide spent fuel based on fundamental thermodynamics, kinetics, and electrochemistry that can be directly integrated into a repository performance assessment model. Because the model is based on fundamental principles, it can be applied with confidence over geologic time scales. The main features of the fuel degradation model discussed in this report are summarized in Figure 27. The one-dimensional electrochemical/reactive transport FMDM was developed to meet this objective. The recent and on-going work described in this report involved quantifying the role that H_2 produced from the anoxic corrosion of steels plays in suppressing the oxidative dissolution of the fuel. To this end, an electrokinetic mixed potential model for steel corrosion was added as a sub-model to the FMDM to calculate the amounts of H_2 generated as various metallic components in a waste package corrode. Sensitivity calculations relating the fuel degradation rate to the steel corrosion rates were performed to identify information gaps that need to be addressed to fully couple, calibrate, and validate the models.

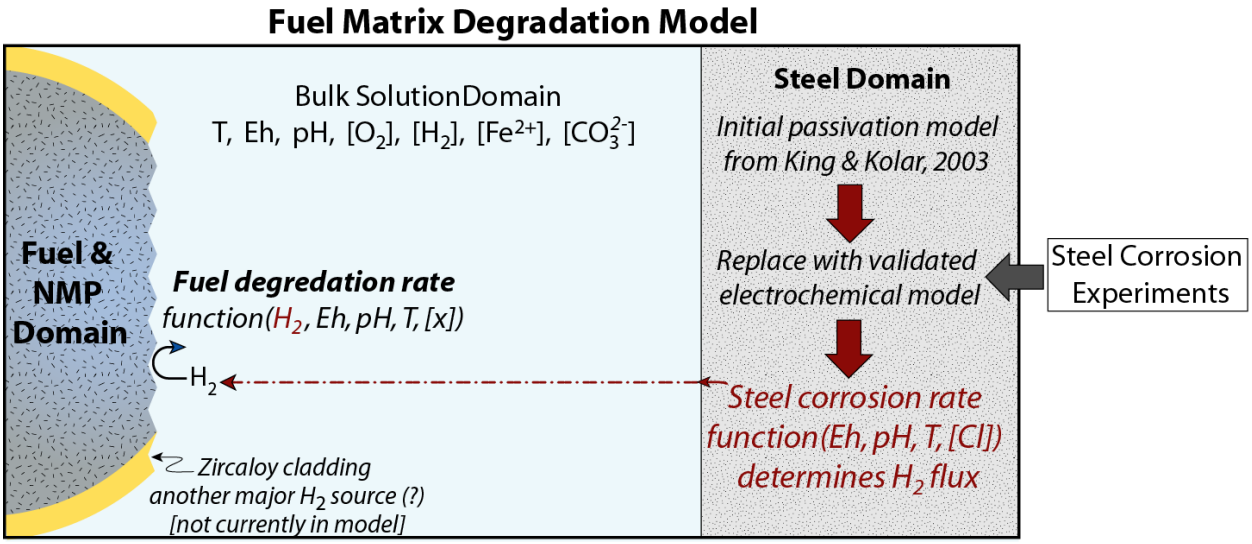

Figure 27. Conceptual summary of the FMDM highlighting the main features discussed in this report.

The accomplishments and conclusions of this study are summarized as follows:

- An electro-kinetic mixed potential model for the corrosion of steels was coupled with the spent fuel dissolution reactions. Modeling steel corrosion is a key part of the FMDM because it represents the main source of H_2 within the breached canister. Previous work has shown that less than 1 mM dissolved H_2 can suppress the oxidative dissolution of spent fuel under anticipated disposal conditions (Jerden et al., 2015, Wu et al., 2014)
- Sensitivity runs with the FMDM and new steel corrosion module show that enough H_2 is produced when the steel is corroding actively to inhibit the oxidative dissolution of the fuel and limit the rate of fuel degradation to the chemical dissolution rate (which is 3 to 4 orders of magnitude lower than the maximum oxidative dissolution rate).

  - Model results indicate lower steel corrosion rates due to passivation of the steel surface will allow for significantly higher spent fuel degradation rates. This is because, under anoxic conditions, the steel corrosion rate is directly proportional to the generation rate of H_2.
  - The amount of H_2 produced during passive steel corrosion is uncertain due to the lack of experimental data on steel corrosion rates in repository-relevant conditions where the Eh and pH are carefully controlled and monitored.

- The FMDM sensitivity runs reveal that, if the fuel-steel reaction-diffusion cell is treated as a relatively open system, the build-up of the amount of H_2 needed to suppress the oxidative dissolution of the fuel occurs relatively slowly and allows faster fuel dissolution during the early time steps of the model. Under closed system conditions, the oxidative dissolution of the fuel can be fully suppressed by corrosion of carbon steel at the rates that are commonly observed (~150 g $m^{-2}\,yr^{-1}$). Given that canister breaches will likely be filled with ferrous corrosion products and given the impervious nature of the surrounding bentonite buffer, the closed-system conditions are representative of disposal conditions.
- The use of U(VI) solubility limits in the FMDM results in formation of a 100 – 1000 μm thick porous layer of alteration products on the fuel surface that leads to an accumulation of H_2 near the fuel surface. This causes a decrease in fuel degradation rates even when the H_2 generation rate (steel corrosion rate) is relatively low. This is due to the tortuosity of the porous U(VI) layer slowing the diffusion of species through the layer leading to H_2 accumulation.
  - It is not yet clear whether this process is real or an artifact of how the U(VI) layer is modeled in the FMDM. Experiments in which the U(VI) alteration layer can be grown under controlled Eh and pH conditions in the presence and absence of H_2 are needed to determine if this is a real phenomenon.
- The FMDM was applied to two simple repository scenarios in which a breached spent fuel canister containing relevant masses of carbon-steel, 316 stainless steel and borated steel were allowed to corrode in a groundwater typical of a crystalline rock repository (Table 4), . Various steel corrosion rates and starting oxidant concentrations were used and the Eh, pH and spent fuel corrosion rates were calculated. The steel corrosion rates were held constant in the simple titration model approach.
  - It was found that the pH evolution is particularly sensitive to the starting O_2 concentration in the solution. If it was assumed that the solution contained ~10 mM O_2 (residual from canister emplacement and/or from the decomposition of radiolytic H_2O_2), the pH decreased from a starting value of 8 down to around 4, and then increased to 9 once the O_2 was consumed. The H^+ consuming and generating reactions responsible for this behavior are identified (Reactions 3 – 8). The initial pH decrease does not occur when the starting O_2 concentration is in the μmolar range.
  - When the FMDM is applied using the steel titration model results, it shows that the fuel degradation rate will increase after carbon steel is consumed during the first few thousand years leading to a decrease in the H_2 concentration and a corresponding increase in the fuel degradation rate. This indicates that canisters containing relatively large amounts of carbon steel will likely provide low radionuclide source terms because they will maintain high H_2 concentrations for longer time periods.
- Comparison of the simple steel corrosion model currently used in the FMDM module with recent electrochemical measurements indicates that model is not sufficient to accurately model long-term fuel degradation. Electrochemical tests are needed to implement an improved steel passivation model in the FMDM by providing data sets with which the model can be calibrated for metals that

will be present in the EBS and for key environmental variables. The model and test protocol developed at ANL for metal waste form degradation are probably suitable, but this should be verified.

- Simulations show how the presence of metals that corrode at different rates can extend the time over which H_2 generation will attenuate the fuel degradation rate. The materials used in the EBS can be selected to benefit the long-term performance of disposed fuel based on their measured corrosion behaviors and impacts on FMDM calculations.
- Preliminary electrochemical tests on the corrosion of Zircaloy-4 cladding suggest that this material will provide another important source of H_2 that is not currently accounted for in the FMDM. Including the H_2 generated during Zircaloy cladding corrosion on fuel degradation will benefit performance assessments. More experimental work is needed to confirm and conceptualize how Zircaloy corrosion could influence spent fuel degradation rates and measure the dependence on environmental variables, particularly the chloride concentrations.

8. REFERENCES

Buck E., Jerden, J., Ebert, W., Wittman, R., "Coupling the Mixed Potential and Radiolysis Models for Used Fuel Degradation," FCRD-UFD-2013-000290, 2013.

Buck, E., Mausolf, E., McNamara, B., Soderquist, C., Schwantes, J., "Nanostructure of Metallic Particles in Light Water Reactor Used Nuclear," *Journal of Nuclear Materials*, vol. 61, pp. 236–243, 2015.

Bethke, C.M., Yeakel, S. "The Geochemist's Workbench User's Guides, Version 10.0," Aqueous Solutions LLC, Champaign, Illinois, 2014.

Caporuscio, F.A., Cheshire, M.C., Rearick, M.S., and Jove-Colon, C. "LANL Argillite EBS Experimental Program 2014," FCRD-USED-2014-000491, 2014.

Caporuscio, F.A., Cheshire, M.C., Palaich, S., Norskog, K., Jove-Colon, C., "Argillite Disposal R&D-LANL 2015. Summary of baseline experiments for generic repository engineered barriers," FCRD-UFD-2015-000356, LA-UR-15-26110, 2015.

Caporuscio, F.A., Norskog, K , Maner, J., Palaich S., Cheshire, M.C., Rearick, M.S., "LANL Argillite EBS Experimental Program 2016," FCRD-UFD-2016-000620, LA-UR-16-25834, 2016.

CRWMS M&O 2003, "In-Package Chemistry Abstraction," ANL-EBS-MD-000037 REV 02., Las Vegas, Nevada: CRWMS M&O. ACC: MOL.20000418.0818, 2003.

Cunnane, J.C., 2004, "CSNF Waste Form Degradation: Summary Abstraction," Bechtel SAIC Company LLC Technical Report, ANL-EBS-MD-000015 REV 02, August 2004.

Debruyn, W., J. Dresselaers, Ph. Vermieren, J. Kelchtermans and H. Tas. "Corrosion of container and infrastructure materials under clay repository conditions," Commission of the European Communities Report, EUR 13667 EN, 1991.

Ebert, W.L. and Gattu, V.K. "Production and Initial Testing of RAW-6 Materials," FCRD-MRWFD-2016-000350, 2016.

Ebert, W.L., Gattu, V.K., and Indacochea, J.E. "A Degradation Model and Testing Protocol for Metallic Waste Forms," NTRD-MRWFD-2017-000189, 2017. (in preparation).

Energy Solutions, "Generic Design for Small Standardized Transportation, Aging and Disposal Canister Systems," DOE Advisory and Assistance Services Contract Task Order 18, UPDATED FINAL REPORT, May 14, 2015, 317 p.

Fillmore, D.L., "Parameter Selection for Department of Energy Spent Nuclear Fuel to be Used in the Yucca Mountain License Application, Idaho National Engineering and Environmental Laboratory Report," INEEL/EXT-03-01032 Revision 1, October 2003

Gattu, V.K., Private Communication. February 18, 2017

Grambow, B., Bruno, J., Duro, L., Merino, J., Tamayo, A., Martin, C., Pepin, G., Schumacher, S., Smidt, O., Ferry, C., Jegou, C., Quiñones, J., Iglesias, E., Rodriguez Villagra, N., Nieto, J., Martínez-

Esparza, A., Loida, A., Metz, V., Kienzler, B., Bracke, G., Pellegrini, D., Mathieu, Wasselin-Trupin, G., Serres, C., Wegen, D., Jonsson, M., Johnson, L., Lemmens, K., Liu, J., Spahiu, K., Ekeroth, E., Casas, I., de Pablo, J., Watson, C., Robinson, P., Hodgkinson, D., "Model Uncertainty for the Mechanism of Dissolution of Spent Fuel in Nuclear Waste Repository," European Commission, Final Report for MICADO Project, EUR 24597, 2010.

JNC "Project to establish the scientific and technical basis for HLW disposal in Japan," Japan Nuclear Cycle Development Institute, Supporting Report 2, Repository Design and Engineering Technology, 2000.

Jerden J. Copple J., Frey K. Ebert W., "Prototype Fortran Version of the Mixed Potential Process Model for Used Fuel Degradation," M4FT-15AN0806012, October 15, 2014

Jerden J., Hammond, G., Copple J., Cruse, T., Ebert W., "Fuel Matrix Degradation Model: Integration with Performance Assessment and Canister Corrosion Model Development," FCRD-UFD-2015-000550, July 21, 2015

Jerden J. Frey K. Ebert W., "A Multiphase Interfacial Model for the Dissolution of Spent Nuclear Fuel, *Journal of Nuclear Materials*, vol. 462, pp. 135–146, 2015.

Johnson J, Anderson F, Parkhurst DL. Database thermo.com.V8.R6.230, Rev 1.11. Lawrence Livermore National Laboratory, Livermore, California; 2000

Johnson, L.H. and F. King, "Canister options for the disposal of spent fuel," Nagra Technical Report 02-11, 2003.

Carter, J., Luptak, A., Gastelum, J., Stockman, C., Miller, A., "Fuel Cycle Potential Waste Inventory for Disposition," FCR&D-USED-2010-000031 Rev 5, July 2012

Kaesche, H., "Metallic Corrosion," National Association of Corrosion Engineers International, Houston, TX, 1985.

King F. and Kolar M., "An Improved C-Steel Corrosion Model For the Mixed-Potential Model for Used Fuel Dissolution (MPM Version 1.4)," Ontario Hydro, Nuclear Waste Management Division Report No: 06619-REP-01300-l0027-R00, 2001.

King F. and Kolar M., "The Mixed-Potential Model for UO_2 Dissolution MPM Versions V1.3 and V1.4," Ontario Hydro, Nuclear Waste Management Division Report No. 06819-REP-01200-10104 R00, 2003.

King, F., "Overview of a Carbon Steel Container Corrosion Model for a Deep Geological Repository in Sedimentary Rock," Nuclear Waste Management Organization Report TR-2007-01, March 2007, 71 p.

Kleykamp, H., "Constitution and Thermodynamics of the Mo-Ru, Mo-Pd, Ru-Pd and Mo-Ru-Pd Systems," *Journal of Nuclear Materials*, vol. 167, pp. 49-63, 1989.

Laaksoharju M., Smellie, J., Tullborg, E-L., Gimeno, M., Hallbek, L., Molinero, J., Waber, N., "Bedrock hydrogeochemistry Forsmark site descriptive modeling SDM-Site Forsmark," SKB R-Report (R-08-47), SKB, Stockholm, Sweden, 2008.

Lanza, F. and C. Ronsecco, "Corrosion of low-carbon steel in clay and sea sediments," Commission of the European Communities Report EUR 10522 EN, 1986.

Mariner, P., Gardner, P., Hammond, G, Sevougian, D, Stein E., "Application of Generic Disposal System Models," FCRD-UFD-2015-000126, SAND2015-10037, September 22, 2015, 209 p.

Marsh, G.P. and K.J. Taylor, "An assessment of carbon steel containers for radioactive waste disposal," Corrosion Science vol. 28, pp. 289-320, 1988

Marsh, G.P., K.J. Taylor, S.M. Sharland, and P.W. Tasker, "An approach for evaluating the general and localized corrosion of carbon-steel containers for nuclear waste disposal," Mat. Res. Soc. Symp. Proc. Vol. 84, Materials Research Society, Pittsburgh, PA, p. 227-238, 1987.

Marsh, G.P., A.H. Harker, and K.J. Taylor, "Corrosion of carbon steel nuclear waste containers in marine sediment," Corrosion vol. 45, pp. 579-589, 1989.

Metz V., Loida A., Bohnert E., Schild D., Dardenne K., "Effects of Hydrogen and Bromide on the Corrosion of Spent Nuclear Fuel and γ-irradiated UO_2(s) in NaCl Brine," *Radiochim. Acta* 96, 637–648, 2008.

Miller, W.M., W.R. Alexander, N.A. Chapman, I.G. McKinley, and J.A.T. Smellie, "Natural analogue studies in the geological disposal of radioactive wastes," Studies in Environmental Sciences 57, Elsevier, Amsterdam (also Nagra Technical Report NTB 93-03), 1994.

Ollila, K., "Dissolution of Unirradiated UO_2 and UO_2 Doped with ^{233}U in Low- and High-Ionic-Strength NaCl Under Anoxic and Reducing Conditions," Posiva Working Report 2008-50, 2008.

Peat, R. S. Brabon, P.A.H. Fennell, A.P. Rance, and N.R. Smart, "Investigation of Eh, pH and corrosion potential of steel in anoxic groundwater," SKB Technical Report TR-01-01, 2001.

Posiva, "Safety case for the disposal of spent nuclear fuel at Olkiluoto – Design Basis 2012," Eurajoki, Finland: Posiva Oy. POSIVA 2012-03. ISBN 978-951-652-184-1, 2012.

Radulescu, G., "Repository Science/Criticality Analysis," Oak Ridge National Laboratory, Reactor and Nuclear Systems Division, FTOR11UF0334, ORNL/LTR-2011, Oak Ridge National Laboratory, Oak Ridge, TN., 2011.

Röllin S., Spahiu K., Eklunda U., "Determination of Dissolution Rates of Spent Fuel in Carbonate Solutions Under Different Redox Conditions with a Flow-through Experiment," *Journal of Nuclear Materials*, vol. 297, pp. 231–243, 2001.

Shoesmith, D., "The Role of Dissolved Hydrogen on the Corrosion/Dissolution of Spent Nuclear Fuel," Nuclear Waste Management Organization, Toronto, Ontario, Canada, TR-2008-19, November 2008.

Simpson, J.P. and P.-H. Valloton, "Experiments on container materials for Swiss high-level waste disposal projects, Part III," Nagra Technical Report 86-25, 1986.

Simpson, J.P. 1989, "Experiments on canister materials for Swiss high- level waste disposal projects, Part IV. National Cooperative for the Storage of Radioactive Waste Technical Report," NAGRA-NTB-89-19, 1989.

Smart, N.R., D.J. Blackwood, and L.O. Werme, "The anaerobic corrosion of carbon steel and cast iron in artificial groundwaters," SKB Technical Report TR-01-22, 2001.

Smart, N.R., D.J. Blackwood, and L.O. Werme, "Anaerobic corrosion of carbon steel and cast iron in artificial groundwaters: Part 1 – electrochemical aspects," Corrosion vol. 58, pp.547-559, 2002.

Wang Y. et al., "Used Fuel Disposal in Crystalline Rocks: Status and FY14 Progress," FCRD-UFD-2014-000060, SAND2014, Sandia National Laboratories, Albuquerque, NM., 2014.

Wu, L., Qina, Z., Shoesmith, D.W., "An improved model for the corrosion of used nuclear fuel inside a failed waste container under permanent disposal conditions," Corrosion Science vol. 84, pp.85–95, 2014.